Author Manuscript
Author Manuscript
Author Manuscript
Author Manuscript

HHS Public Access
Author manuscript
Cell Rep. Author manuscript; available in PMC 2024 November 08.

Published in final edited form as:
Cell Rep. 2024 October 22; 43(10): 114747. doi:10.1016/j.celrep.2024.114747.

Regulation of synapse density by Pumilio RNA-binding proteins

Lisa K. Randolph[1], **Michaela M. Pauers**[1], **José C. Martínez**[2,3], **Leslie J. Sibener**[1], **Michael A. Zrzavy**[4], **Nyle A. Sharif**[4], **Tatiana M. Gonzalez**[5], **Kapil V. Ramachandran**[4,6,7], **Daniel Dominguez**[2,8,9,10], **Ulrich Hengst**[4,11,12,*]

[1]Doctoral Program in Neurobiology and Behavior, Columbia University, New York, NY 10032, USA

[2]Lineberger Comprehensive Cancer Center, University of North Carolina at Chapel Hill, Chapel Hill, NC 27599, USA

[3]Division of Hematology, Department of Medicine, School of Medicine, University of North Carolina at Chapel Hill, Chapel Hill, NC 27599, USA

[4]Taub Institute for Research on Alzheimer's Disease and the Aging Brain, Columbia University Vagelos College of Physicians and Surgeons, New York, NY 10032, USA

[5]Integrated Program in Cellular, Molecular and Biomedical Studies, Columbia University Vagelos College of Physicians and Surgeons, New York, NY 10032, USA

[6]Department of Neurology, Columbia University Vagelos College of Physicians and Surgeons, New York, NY 10032, USA

[7]Department of Neuroscience, Columbia University Vagelos College of Physicians and Surgeons, New York, NY 10032, USA

[8]Curriculum in Bioinformatics and Computational Biology, University of North Carolina, Chapel Hill, NC 27599, USA

[9]Department of Pharmacology, University of North Carolina at Chapel Hill, Chapel Hill, NC 27599, USA

[10]RNA Discovery Center, University of North Carolina, Chapel Hill, NC 27599, USA

[11]Department of Pathology and Cell Biology, Columbia University Vagelos College of Physicians and Surgeons, New York, NY 10032, USA

[12]Lead contact

This is an open access article under the CC BY-NC-ND license (https://creativecommons.org/licenses/by-nc-nd/4.0/).

*Correspondence: uh2112@cumc.columbia.edu.

AUTHOR CONTRIBUTIONS

Conceptualization, L.K.R. and U.H.; methodology, L.K.R., M.M.P., K.V.R., U.H., J.C.M., and D.D.; experimental investigation, L.K.R., M.M.P., M.A.Z., and T.M.G.; RNA-seq and iCLIP analysis, J.C.M.; calcium imaging acquisition, L.K.R. and N.A.S.; calcium imaging analysis, L.J.S.; writing – original draft, L.K.R. and U.H.; writing – review & editing, L.K.R., U.H., and J.C.M.; funding acquisition, L.K.R., K.V.R., and U.H.; supervision, U.H.

DECLARATION OF INTERESTS

The authors declare no competing interests.

SUPPLEMENTAL INFORMATION

Supplemental information can be found online at https://doi.org/10.1016/j.celrep.2024.114747.

Author Manuscript Author Manuscript Author Manuscript Author Manuscript

Abstract

The formation, stabilization, and elimination of synapses are tightly regulated during neural development and into adulthood. Pumilio RNA-binding proteins regulate the translation and localization of many synaptic mRNAs and are developmentally downregulated in the brain. We found that simultaneous downregulation of Pumilio 1 and 2 increases both excitatory and inhibitory synapse density in primary hippocampal neurons and promotes synapse maturation. Loss of Pum1 and Pum2 in the mouse brain was associated with an increase in mRNAs involved in mitochondrial function and synaptic translation. These findings reveal a role for developmental Pumilio downregulation as a permissive step in the maturation of synapses and suggest that modulation of Pumilio levels is a cell-intrinsic mechanism by which neurons tune their capacity for synapse stabilization.

In brief

Pumilio RNA-binding proteins are developmentally downregulated in the brain. Randolph et al. report that the simultaneous downregulation of Pumilio 1 and 2 promotes synapse maturation and increases the density of excitatory and inhibitory synapses. Thus, the regulation of Pumilio protein levels represents a cell-intrinsic mechanism for the modulation of synapse maturation.

Graphical Abstract

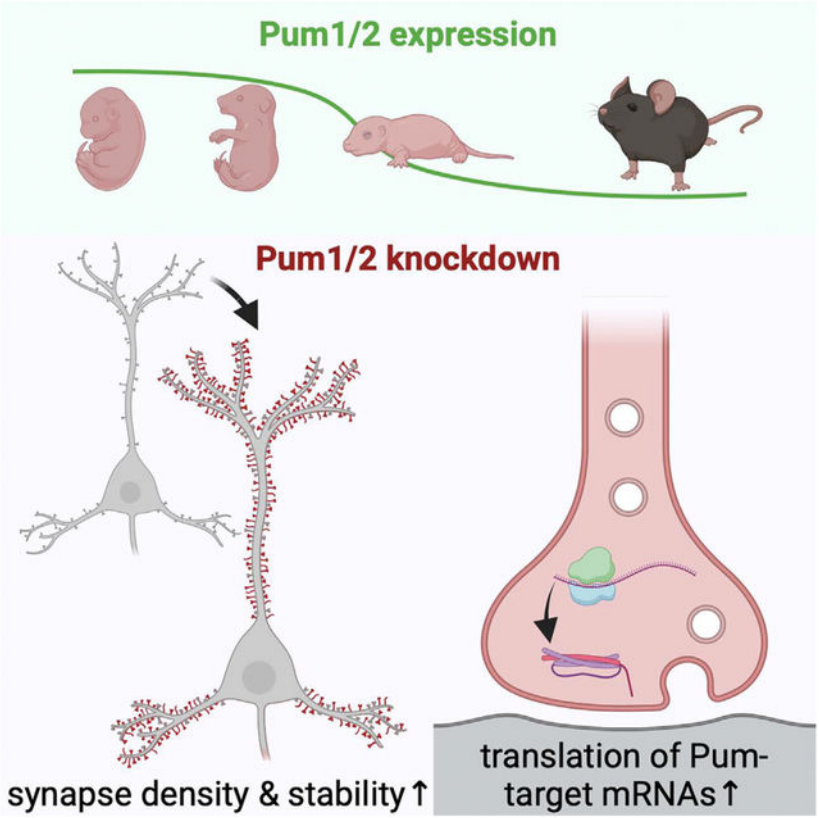

Author Manuscript Author Manuscript Author Manuscript Author Manuscript

INTRODUCTION

Neurons are among the most morphologically complex, dynamic, and long-lived cells. Consequently, neuronal gene expression must be tightly regulated both spatially and temporally. RNA-binding proteins (RBPs) contribute to this precise regulation by controlling mRNA transport, translation, and stability.[1,2]

Coordinated RNA regulation is especially important for highly sensitive processes such as synapse formation and stabilization. New protein synthesis is required for long-term potentiation,[3–5] including the dendritic synthesis of CaMKIIα,[6–8] Arc,[9–12] and BDNF.[13] Presynaptic protein synthesis is required for inhibitory long-term depression,[14] and presynaptic β-catenin synthesis modulates vesicle release.[15] Additionally, we have previously reported that axonal synthesis of synaptosomal-associated protein 25 (SNAP-25) is required for presynaptic terminal formation and regulates vesicle release.[16]

Despite tremendous progress in defining the significance of spatially and temporally restricted protein synthesis in neurons, much remains unknown about the molecular machinery governing how the neuronal transcriptome is dynamically regulated to support distinct functions across developmental stages. We have previously reported that the presence of one or more Pumilio-binding elements (UGUAHAUA) in the 3′ UTR prevents the localization of mRNAs into developing axons due to the retention of the transcripts in the cell body by the RBP Pumilio 2 (Pum2).[17] An intriguing implication of these findings is that developmental changes in the expression of RBPs, such as Pumilios, might permit the transport and/or translation of their target mRNAs only at certain times, thereby matching the local transcriptome to changing demands. Indeed, Pumilio expression is reduced once axons complete their phase of rapid growth and start forming synapses.[17,18] This developmental drop in Pumilio expression in the mouse brain is accompanied by increased localization of Pumilio targets into axons.[17] The presynaptic transcriptome in adult *C. elegans* is also enriched for Pumilio target mRNAs.[19]

Most studies to date have focused on the roles of Pum1 and Pum2 individually. However, Pum1 and Pum2 regulate each other's expression and share nearly 700 mRNA targets.[18] Conditional neural loss of both Pum1 and Pum2 leads to impairments in neurogenesis, learning, and memory.[18] Furthermore, Pum1 and Pum2 share similar developmental expression profiles, with both proteins being highly expressed in the mouse brain in early development and substantially downregulated by post-natal day (P)15–P30.[18] To determine the function of their developmental downregulation, we simultaneously knocked down Pum1 and Pum2 in hippocampal neurons and found that the loss of both Pumilios increases synapse density across multiple stages of neuronal maturation and specifically increases the number of mature synapses. Conversely, individual downregulation of Pum1 or Pum2 reduces synapse density. Our results reveal that Pumilios are important regulators of synapse stability and maturation and highlight the importance of studying the function of RBPs in the context of their own regulatory networks.

Author Manuscript Author Manuscript Author Manuscript Author Manuscript

RESULTS

Pum1 and Pum2 targets are developmentally regulated

To gain insight into the expression and regulation of Pum1 and Pum2 and their RNA targets throughout neurodevelopment, we analyzed RNA sequencing data from various developmental stages in the mouse cortex.[20] Consistent with previous findings,[17,18,20] we observed a significant shift in cortical gene expression around P7 (Figure S1A) and a decrease in Pum1 and Pum2 mRNA levels throughout neurodevelopment (Figure 1A). We next investigated the developmental expression of shared RNA targets of Pum1 and Pum2, which we identified by analyzing an iCLIP dataset from neonatal mouse cortex.[18] Consistent with an established function of Pumilio proteins as negative regulators of translation, the overall expression of our identified shared Pum1 and Pum2 targets increased across neurodevelopment and peaked at P7 (Figure 1A), a time when cortical neurons switch their program to synapse formation.[20]

To understand if developmental Pumilio downregulation is a neuron-intrinsic mechanism, we measured Pumilio protein levels over time in cultured primary rat hippocampal neurons. Both Pum1 and Pum2 were significantly downregulated over the course of 21 days *in vitro* (DIV), averaging at least a 50% reduction in protein levels from DIV6 to DIV21, suggesting that this is a cell-autonomous process (Figure 1B).

Individual Pum1 or Pum2 knockdown reduces synapse density

To investigate whether the downregulation of Pumilio proteins affects synapse density, we suppressed Pum1 or Pum2 expression individually using short hairpin RNAs (shRNAs) delivered by lentivirus at DIV2 (Figure S1B). As *Pum1* and *Pum2* mRNAs contain several Pumilio binding elements and regulate each other's expression, there is a modest but statistically non-significant increase in one Pumilio paralog when the other is reduced (Figure S1B).

At DIV14–DIV15, when cultured neurons have begun to establish mature synapses, we assessed the number of synapses by measuring the juxtaposition between the presynaptic marker synapsin I (Syn-I) and the excitatory postsynaptic marker postsynaptic density protein 95 (PSD-95).[21,22] Knockdown of either Pum1 or Pum2 dramatically reduced excitatory synapse density (Figures 1C and 1D).

Dual Pumilio knockdown increases synapse density

Because both Pumilio paralogs are downregulated in parallel during neuronal maturation, we investigated the effect of simultaneously downregulating both Pum1 and Pum2 by designing an shRNA, shPum, that targets a homologous region of the rat *Pum1* and *Pum2* mRNAs (Figures S1C and S1F). In contrast to individual knockdown, the synaptic density of shPum neurons at DIV14–DIV15 was significantly increased (Figures 1E and 1F). The same effect was observed when we combined the two shRNAs previously used for single knockdown into the same construct (shPum1-shPum2) (Figures S1D and S1E).

Author Manuscript Author Manuscript Author Manuscript Author Manuscript

To test whether the loss of either Pum1 or Pum2 function was largely responsible for the increase in synaptic density, we knocked down both Pumilios with shPum and co-expressed a rescue construct ($Pum1^R$ or $Pum2^R$) (Figures S1F and S1G). Restoring Pum2, but not Pum1, levels reversed the increase in synapse density (Figures 1G and 1H), indicating that specifically the downregulation of Pum2 is required for the increase in synapses upon dual Pumilio knockdown, although this does not rule out a role for Pum1.

Dual Pumilio downregulation increases dendritic spine density but not dendrite complexity

As Pum2 regulates dendrite morphogenesis and arborization,[23–25] the upregulation of synapses seen in shPum neurons could be due to altered dendritic architecture. Analysis of dendrite complexity by Sholl analysis[26] revealed that knockdown of Pum2 individually caused an increase in short dendrites (Figure 2A), which is consistent with previous findings,[24] while there was no effect of Pum1 knockdown. There was no significant difference between shControl and shPum dendrites (Figure 2B).

To determine if dendritic spines were affected, we co-stained neurons with MAP2 and phalloidin to label microtubules and actin structures. Dendritic spines were apparent in both MAP2 and phalloidin channels, and the MAP2 channel was selected for quantification due to its enhanced signal-to-noise ratio. We found that dendritic spine density was significantly increased in shPum neurons, consistent with an increase in synapse density, while the length of dendritic spines was not affected (Figure 2C).

Dual Pumilio knockdown drives increased synapse maturation

Next, we asked whether dual Pumilio downregulation drives premature synapse formation or enhanced maturation and stabilization of nascent synapses by assessing synapse density in shControl vs. shPum neurons at five time points over the course of 21 days. Both Pum1 and Pum2 levels were significantly reduced by DIV8 (Figure S2A). Synapse density progressed normally in shPum neurons at early time points (DIV6–DIV11) but surpassed shControl levels at DIV15 and to an even greater extent at DIV21 (Figures 3A and 3B), indicating that dual Pumilio downregulation does not trigger premature synapse formation but instead increases the overall density of synapses after the onset of synaptogenesis. To directly test the role of Pumilios in regulating synapse density at late stages of neuronal maturation, we infected neurons with shRNA-expressing lentiviruses at a late time point (DIV15) and performed the synapse density analysis at DIV21. In contrast to the marked reduction in synapses observed when Pum1 or Pum2 are knocked down individually at early time points, there was no effect of either shPum1 or shPum2 when cells were infected on DIV15 (Figures 3C, 3D, and S2B). However, dual Pumilio knockdown at DIV15 again resulted in a significant increase in synapse density at DIV21 (Figures 3E, 3F, and S2C).

To assess the effect of Pumilio downregulation on synapse maturation, we treated neurons with latrunculin A (LatA) to depolymerize F-actin. LatA specifically destabilizes immature, but not mature, synapses.[27] LatA treatment reduced the percentage of the area covered by Syn-I+ puncta in both shControl and shPum neurons, but shPum neurons still had significantly more Syn-I+ area than shControl neurons after LatA treatment (Figures 3G

Author Manuscript Author Manuscript Author Manuscript Author Manuscript

and 3H). Together, these results indicate that dual Pumilio downregulation increases synapse density by driving an increase in synapse maturation.

Dual Pumilio downregulation increases both excitatory and inhibitory synaptic density

To determine whether inhibitory synapses are also affected by Pumilio downregulation, we measured the co-localization of the vesicular GABA transporter (VGAT) and gephyrin. shPum treatment led to a significant increase in inhibitory synapses, and the average size of gephyrin puncta was also modestly increased (Figure 4A). Gephyrin cluster size is associated with increased maturity of inhibitory synapses,[28] again supporting a role for Pumilios in synapse maturation. We next directly compared the number of excitatory and inhibitory presynaptic puncta using the vesicular glutamate transporter 1 (VGLUT1) and VGAT in the same optical field. Both VGLUT1 and VGAT were significantly upregulated by shPum, and the VGLUT1/VGAT ratio was significantly decreased (Figure 4B), indicating a larger increase in inhibitory vs. excitatory synapses. Baseline firing rates of shPum neurons were not affected as measured by live calcium imaging (Figures S3A and S3B), although this does not rule out the possibility that more subtle aspects of synaptic activity are altered.

Synaptic gene regulation by Pum1 and Pum2

To elucidate the specific gene classes regulated by Pum1 and Pum2 that might account for the synaptic phenotypes observed, we conducted Gene Ontology analysis on the neonatal cortical iCLIP Pum1/2 targets that we previously identified (Figure 1A). This analysis revealed a notable enrichment of genes involved in axonogenesis, synapse organization, and synapse structure (Figure 4C). Further analysis of shared Pum1/2 targets using SynGO[29] highlighted significant enrichment in synaptic terms, encompassing both postsynaptic and presynaptic processes, such as postsynaptic specialization and presynaptic active zone (Figure 4D).

We next examined RNA sequencing data from mice with either Pum1, Pum2, or *Nestin*-Cre-mediated conditional double knockout (Ndcko).[18] Consistent with prior reports, single knockout of Pum1 or Pum2 did not significantly alter global gene expression.[17,30,31] Conditional double knockout resulted in notable changes to the transcriptome (Figure S4A), including an activation of mitochondrial processes and a suppression of axonal development (Figure 4E). While genes involved in synapse assembly were suppressed, genes involved in synaptic translation were upregulated. Approximately 15% of the differentially expressed genes in this dataset were direct targets of both Pum1 and Pum2 identified in our iCLIP analysis. This significant, yet partial, overlap suggests that while Pumilios play a direct post-transcriptional regulatory role, there are likely additional, indirect changes in gene expression.

To investigate the regulation of an individual synaptic Pumilio target mRNA target, we focused on *Snap25* because of its importance for presynaptic terminal differentiation,[16] identification as a target of Pum1 and Pum2,[18] and role at both excitatory and inhibitory synapses. RNA immunoprecipitation (RIP) from embryonic day (E)17 rat cortex confirmed the interaction of Pum1 and Pum2 with *Snap25* mRNA (Figure S4B). Although we did not observe significant changes in the global mRNA or protein levels of *Snap25* or three

Author Manuscript Author Manuscript Author Manuscript Author Manuscript

additional synaptic Pumilio targets (*L1cam, Syt1,* and *Nrxn1*) with dual Pumilio knockdown (Figures S4C and S4D), puromycin labeling coupled with proximity ligation assay (puro-PLA)[32] revealed significantly elevated *Snap25* translation (Figures S4E and S4F). Over 85% of SNAP-25 puro-PLA puncta localized to neurites, and translational events in neurites were also significantly increased by shPum (Figure S4F). Pumilios regulate large sets of mRNAs and likely exert their effects at the synapse by coordinated changes in the translation and subcellular localization of many of the target genes identified in our analysis. Increased synthesis of SNAP-25 represents one potential mechanism among these by which dual Pumilio downregulation may enhance synapse stability.

DISCUSSION

We demonstrate that dual Pumilio downregulation increases excitatory and inhibitory synapses in cultured hippocampal neurons specifically at late stages due to enhanced synaptic stabilization and maturation. We also find that Pumilio downregulation impacts synapses differently depending on whether they are downregulated individually or in parallel. One possible explanation for this is that the decrease in synapses observed with individual knockdown is driven primarily by overcompensation of the paralog Pumilio. An alternate possibility is that these differing effects are due to differential disruption of the network of Pumilio-interacting proteins. The Pumilio interactome varies among brain regions and neuronal subtypes.[33,34] A mild reduction of Pum1 disrupts only the expression of Pum1 targets, while more severe reductions also affect the expression of Pum1-interacting proteins.[34] Lowering the levels of either one or both Pumilio proteins could perturb the network of interacting proteins in different ways that produce divergent downstream effects.

Dual Pumilio knockdown increased both excitatory and inhibitory synapses, with a greater effect on inhibitory synapses. Pum2 knockdown increases miniature excitatory postsynaptic current (mEPSC) frequency[24,35] and decreases miniature inhibitory postsynaptic current (mIPSC) amplitude,[30] and reductions in Pum2 are associated with hyperexcitability and seizure.[24,36–39] While we did not detect any global changes in neural activity, further investigation will be required to determine the more subtle effects of dual Pumilio knockdown on synaptic transmission, plasticity, or the overall balance of excitation to inhibition.

The precise mechanisms by which Pumilios regulate synapse density are still uncertain. Pumilio proteins regulate mRNA targets on many different levels, including translational repression,[40,41] degradation,[42–45] translational activation,[30,40,46,47] and localization.[17,48–50] We identified synapse organization as one of the top categories of Pumilio mRNA targets, and genes involved in translation at the synapse and mitochondrial function are significantly upregulated in the Pum1/2 knockout brain. Mitochondria play a critical role in the presynaptic terminal for energy production and calcium buffering[51,52] and supply the energy required for local translation at the dendritic spine during synaptic plasticity.[53] Mature synapses in the calyx of Held are dependent on mitochondrial oxidative phosphorylation for ATP production, while immature synapses can also use glycolysis.[54] The upregulation of nuclear-encoded mitochondrial mRNAs resulting from a reduction of Pumilio proteins may serve as an important step in the developmental shift to mature synapses.

Author Manuscript Author Manuscript Author Manuscript Author Manuscript

We identified over 4,000 mRNAs with significantly altered expression after dual Pumilio knockout, 15% of which were direct, iCLIP-validated shared Pum1/2 targets. The remaining mRNAs may be subject to secondary regulatory events in which direct targets of Pum1 and Pum2 impact the expression of other genes. For example, Pum1 and Pum2 target *Fmr1* mRNA,[18] encoding the RBP FMRP, which has over 800 of its own mRNA targets.[55] Such secondary events could contribute to the observed phenotypes and further underscore the complex regulatory network influenced by Pumilio proteins.

Translation of at least one synaptic Pum1/2 target, *Snap25*, is increased upon dual Pumilio downregulation. Previously, we reported that small amounts of locally synthesized SNAP-25 are critical for synapse assembly and synaptic transmission.[16] As SNAP-25 is a pan-presynaptic protein and both excitatory and inhibitory synapses are affected by Pumilio downregulation, this presents the intriguing notion that local SNAP-25 regulation might be one mechanism by which Pumilios regulate synapse density.

In summary, we report a cell-autonomous mechanism for the regulation of synapse density in which the developmental reduction of Pumilio serves as a permissive step in promoting synapse maturation. Beyond development, these mechanisms may additionally have relevance in aging, which is characterized by synaptic reorganization,[56–58] as Pum2 is upregulated in the aging brain,[59] and Pum2 hyperactivity is associated with an aging phenotype.[60] Thus, Pumilio regulation may represent an important mechanism by which neurons modulate their ability to stabilize synapses in a cell-autonomous manner at various stages throughout the lifespan.

Limitations of the study

We report that the parallel downregulation of Pum1 and Pum2 promotes synapse maturation in developing neurons and that Pumilio mRNA targets are enriched for synaptic genes. Further work will be required to establish a causal relationship between specific Pumilio targets and synaptic phenotypes. Additionally, all experimental manipulations in this study are done in primary rat neurons. Further work in *in vivo* models will be required to determine the generalizability of this mechanism.

RESOURCE AVAILABILITY

Lead contact

Further information and requests for resources and reagents should be directed to and will be fulfilled by the lead contact, Ulrich Hengst (uh2112@cumc.columbia.edu).

Materials availability

All unique reagents generated in this study are available upon request from the lead contact without restriction.

Data and code availability

- This paper analyzes existing, publicly available data. The accession numbers for these datasets are listed in the key resources table.

Author Manuscript Author Manuscript Author Manuscript Author Manuscript

- All original code has been deposited on GitHub and is publicly available as of the date of publication. DOIs are listed in the key resources table.
- Any additional information required to reanalyze the data reported in this work paper is available from the lead contact upon request.

STAR★METHODS

EXPERIMENTAL MODEL AND STUDY PARTICIPANT DETAILS

Rat primary hippocampal neuronal culture—Pregnant Sprague-Dawley rats (*Rattus norvegicus*) were obtained from Envigo (Indianapolis, IN) and housed at the barrier facility at the Columbia University Institute of Comparative Medicine. All rodent procedures were approved by the Columbia University Institutional Animal Care and Use Committee. Pregnant rats were euthanized on embryonic day 17 (E17) by gas displacement with CO_2 at 8 L min^{-1} for at least 9 min, or until there were no signs of breathing for at least 1 min. Bilateral thoracotomy was used as a form of secondary euthanasia. Embryos were removed from the uterus, decapitated, and brains were dissected to extract the hippocampus. As it is not possible to distinguish between male and female embryos at this stage, hippocampi from all embryos in each litter were pooled and all cultures consist of a mix of male and female neurons. Thus, we do not expect the effects we report to be specific to only one sex.

Hippocampi from brains of E17 embryos were subsequently incubated in TrypLE Express (Thermo Fisher Scientific, Waltham, MA) at 37°C for 20 min. TrypLE Express was removed and hippocampi were washed twice with Hank's Balanced Salt Solution (Thermo Fisher Scientific, Waltham, MA) and resuspended in pre-warmed plating medium. Hippocampi were dissociated by gentle trituration with a p1000 pipette tip followed by a p200 pipette tip (30x each tip). After dissociation, cells were passed through a 40 μm cell strainer (Fisher Scientific, Waltham, MA) then centrifuged at 800 rpm for 5 min at room temperature. Cells were resuspended in 300 μL pre-warmed plating medium and counted using C-Chip disposable hemacytometers (INCYTO, Republic of Korea) with Trypan Blue (Thermo Fisher Scientific, Waltham, MA) to indicate cell viability. Laminin solution was aspirated from culture plates and replaced with neurons suspended in plating medium at an experiment-dependent density. Neurons were then cultured in a humidified incubator at 37°C and 5% CO_2. CytoOne multiwell plates (USA Scientific, Ocala, FL) were used in most cases. Sterile ddH_2O was added to the inter-well/perimeter space to prevent evaporation of culture medium over the duration of the culture. On day *in vitro* (DIV) 1, plating medium was aspirated and replaced with growth medium (1X B-27 supplement, 2 mM L-glutamine in Neurobasal; all reagents from Thermo Fisher Scientific, Waltham, MA). On DIV3–4, half of the medium was replaced with fresh growth medium containing 20 μM 5-fluoro-2′-deoxyuridine and 20 μM uridine (FdU/U) (Sigma-Aldrich, St. Louis, MO) to prevent glial proliferation. Every 3–4 days thereafter, half of the medium was replaced with fresh growth medium containing 10 μM FdU/U. Sterile ddH_2O was added to the inter-well/perimeter space every 7 days to prevent evaporation for long-term cultures.

Author Manuscript Author Manuscript Author Manuscript Author Manuscript

METHOD DETAILS

Neuronal culture preparation—Glass coverslips (Carolina Biological Supply, Burlington, NC) were autoclaved, rinsed twice with sterile water, then coated in 0.01 mg mL^{-1} poly-D-lysine (Sigma-Aldrich, St. Louis, MO) in borate buffer (10 mM boric acid, pH 8.4) overnight at 37°C. Alternately, sterile plastic multiwell plates were coated directly with 0.01 mg mL^{-1} poly-D-lysine in borate buffer. Plates or coverslips were washed three times with sterile water, allowed to air dry, then coated with 2 μg mL^{-1} mouse laminin I (R&D Systems, Minneapolis, MN) in plating medium (10% fetal bovine serum, 2 mM L-glutamine, 100 U ml^{-1} penicillin-streptomycin, 1 mM sodium pyruvate in Neurobasal; all reagents from Thermo Fisher Scientific, Waltham, MA) overnight at 37°C.

DNA constructs—Lentivirus expression plasmids with shERWOOD-UltramiR short hairpin RNAs (shRNAs) targeting Rattus norvegicus *Pum1, Pum2*, a homologous region of *Pum1* and *Pum2* (shPum), or a control shRNA targeting the SV40 promoter were obtained from transOMIC Technologies (Huntsville, AL). *Pum1*-and *Pum2*-targeting shRNA constructs were designed using algorithms that enhance potency and specificity.[77,78] shPum dual-targeting hairpin was a custom design. Hairpin sequences were as follows with capital letters indicating the gene-targeting region of the sequence:

shControl:

tgctgttgacagtgagcgAAGGCAGAAGTATGCAAAGCATtagtgaagccacagatgtaATGCTTTGCATACTTCTGCCTGtgcctactgcctcgga;

shPum1:

tgctgttgacagtgagcgcGGGATTGATGCAGACGTCAAAtagtgaagccacagatgtaTTTGACGTCTGCATCAATCCCatgcctactgcctcgga;

shPum2:

tgctgttgacagtgagcgcGCGAATAAACCACTTGTTGAAtagtgaagccacagatgtaTTCAACAAGTGGTTTATTCGCttgcctactgcctcgga;

shPum:

tgctgttgacagtgagcgaTGCCTTATACACCATGATGAAtagtgaagccacagatgtaTTCATCATGGTGTATAAGGCActgcctactgcctcgga.

Plasmids were modified in-house when necessary using In-Fusion cloning technology (Takara Bio, San Jose, CA) to replace the mCMV promoter with the hUbC promoter for enhanced expression in primary neurons, to replace the ZsGreen1-IRES-Puromycin resistance cassette with eGFP or mLumin as an expression marker for certain experiments, or to insert the *Pum1*-and *Pum2*-targeting shRNAs into the same plasmid. For overexpression, FUGW plasmid[62] was used as a backbone (#14883, Addgene, Watertown, MA). In-Fusion cloning technology was used to replace eGFP in FUGW with mouse Pum1 or Pum2 constructs with five silent mutations in the shPum-targeting site to rescue

Author Manuscript Author Manuscript Author Manuscript Author Manuscript

Pum1 or Pum2 levels. Plasmids were purified using QIAprep Spin Miniprep Kit (Qiagen, Germantown, MD) or ZymoPURE II Plasmid Midiprep Kit (Zymo Research, Irvine, CA).

Lentivirus preparation and infection—HEK293T cells (ATCC, Manassas, VA) or Lenti-X 293T cells (Takara Bio, San Jose, CA) were transfected at 70–99% confluency with 7.5 μg lentiviral expression plasmid, 5.25 μg packaging plasmid (pCMV ΔR8.9), and 2.25 μg envelope plasmid (pHCMV VSVg)[62] in a 10-cm plate or 75-cm flask using Lipofectamine 3000 (Thermo Fisher Scientific, Waltham, MA) according to the manufacturer's instructions. pCMV ΔR8.9, pHCMV VSVg, and FUGW plasmids were generous gifts from David Baltimore. 14–16 h post-transfection, medium was completely changed to 5–6 mL pre-warmed neuronal growth medium after one brief wash with growth medium. 24–36 h after changing the medium, the medium (viral supernatant) was collected, centrifuged at 2000 rpm for 10 min at room temperature, then filtered through a 0.45 μm polyethersulfone (PES) syringe filter (Thermo Fisher Scientific, Waltham, MA). Viruses were aliquoted into cryotubes and stored at −80°C. Viral titers were calculated using the qPCR Lentivius Titer Kit (Applied Biological Materials, Richmond, Canada) according to the manufacturer's instructions. When necessary, lentiviruses were concentrated using the Lenti-X Concentrator kit (Takara Bio, San Jose, CA). Primary hippocampal neurons were infected at an MOI of 5–30 on DIV1 for shRNA knockdown or MOI of 1 on DIV1 for expression of rescue constructs to achieve more than 90% infectivity. Knockdown and proper dosage were verified by Western blot for every virus batch.

Latrunculin A treatment—Primary rat hippocampal neurons were plated at a density of 80,000 cells/well on 18 mm glass coverslips (thickness 0.13–0.17 mm) (VWR, Radnor, PA) in 12-well plates. On DIV1, cells were transduced with shControl or shPum lentiviruses. On DIV18, cells were treated with 2.5 μM latrunculin A (Tocris, Minneapolis, MN) in DMSO or DMSO alone for 24 h, then fixed, stained, and imaged as described below. For image analysis, the eGFP channel was thresholded using the Huang threshold[79] and the area was measured for normalization. The Syn-I channel was thresholded manually for optimal identification of puncta with minimal background signal. Comparable threshold settings were used across all images in the same replicate. Output values for the total area covered by the Syn-I threshold were recorded and then normalized by dividing by the total area of the eGFP cell mask obtained previously.

Protein isolation and western blotting—Primary rat hippocampal neurons were plated at a density of 100,000–200,000 cells/well in poly-D-lysine- and laminin-coated 12-well plates and cultured for 6–21 days. Cells were washed twice in 2 mL ice-cold DPBS containing calcium and magnesium (Thermo Fisher Scientific, Waltham, MA) and then lysed by scraping on ice in 25 μL ice-cold RIPA buffer (Thermo Fisher Scientific, Waltham, MA) containing 1x Halt Protease and Phosphatase Inhibitor Cocktail (Thermo Fisher Scientific, Waltham, MA). Samples were collected and transferred to microcentrifuge tubes. If not proceeding immediately to sample preparation, samples were snap-frozen in liquid nitrogen and stored at −80°C. Otherwise, samples were incubated for 30 min at 4°C with rotation, then centrifuged at maximum speed for 10 min at 4°C. Supernatant was removed to a new tube on ice and pellet was discarded. Total protein concentration was measured using

Author Manuscript Author Manuscript Author Manuscript Author Manuscript

the Pierce BCA Protein Assay Kit (Thermo Fisher Scientific, Waltham, MA) by reading absorbance at 562 nm. Samples were prepared for Western blotting at final concentration of 0.25–0.5 μg μL^{-1} protein in 1x Laemmli buffer (Bio-Rad, Hercules, CA), 2.5%–5% β-Mercaptoethanol, and RIPA buffer (containing Halt inhibitors).

Immediately before running gels, samples prepared in Laemmli buffer were heated at 95°C for 5 min, cooled to room temperature, and briefly centrifuged. 20 μL of samples were loaded into NuPAGE Bis-Tris gels (Thermo Fisher Scientific, Waltham, MA) for a total of 5–10 μg protein per well. Gels were run in NuPAGE MOPS SDS running buffer (Thermo Fisher Scientific, Waltham, MA) containing a 1:400 dilution of NuPAGE antioxidant (Thermo Fisher Scientific, Waltham, MA) in the upper buffer chamber. Gels were run for 30 min at 65 V, followed by 1 h at 165 V. Gels were removed from gel cassettes and proteins were transferred onto 0.45 μm nitrocellulose membranes for 1.5 h at 90 V in cold transfer buffer (25 mM Tris, 192 mM glycine, 20% methanol). Membranes were washed briefly in TBS-T (0.1% Tween 20 in Tris-buffered saline) then incubated in blocking buffer (2% bovine serum albumin in TBS-T) for 1 h at room temperature on a rocker. Membranes were incubated overnight at 4°C on a rocker with primary antibodies diluted in blocking buffer. Primary antibodies and concentrations are listed in the key resources table.

After primary antibody incubation, membranes were washed three times for 10 min in TBS-T, then incubated with HRP-conjugated secondary antibodies (Thermo Fisher Scientific, Waltham, MA) at 1:10,000 in blocking buffer for 1 h at room temperature on a rocker. Membranes were again washed three times for 10 min in TBS-T, then developed with 1-Shot Digital ECL (Kindle Biosciences, Greenwich, CT) for 1 min at room temperature on a rocker and imaged using the KwikQuant Imager (Kindle Biosciences, Greenwich, CT).

Western blotting quantification—For analysis, images in JPEG format were opened in Fiji,[63] converted to 8-bit, and inverted. The gel analyzer tool was used to draw a rectangle around each band of interest and subsequently measure intensity. Intensity peaks were gated by drawing a line across the bottom to close the curve. The area under the curve was then measured. Intensity values for the antibody of interest were normalized by dividing by the intensity of the β-III-tubulin signal in the corresponding lane from the same membrane. Fold change was then calculated by dividing each value by the corresponding control value. For statistical analysis, a one-sample t test was performed to compare to a hypothetical value of 1 representing the control condition.

Immunofluorescence—Primary rat hippocampal neurons were plated at a density of 60,000–80,000 cells/well on 18 mm glass coverslips (thickness 0.13–0.17 mm) (VWR, Radnor, PA) in 12-well plates and cultured for 6–21 days. Cells were rinsed twice quickly with warm DPBS containing calcium and magnesium (Thermo Fisher Scientific, Waltham, MA) and then fixed with 4% paraformaldehyde (PFA) in cytoskeletal preservation buffer (10 mM MES, 138 mM KCl, 3 mM $MgCl_2$, 2 mM EGTA, 320 mM sucrose, pH 6.1) for 20 min at room temperature. PFA was washed off briefly with phosphate-buffered saline (PBS) and coverslips were either stained immediately or stored briefly in PBS at 4°C for later processing. Fixed cells were washed three times for 5 min in PBS, then permeabilized with 0.3% Triton X-100 for 5 min. Triton X-100 was removed with two brief washes in

Author Manuscript Author Manuscript Author Manuscript Author Manuscript

PBS, then coverslips were incubated for 30 min at room temperature in blocking buffer (5% BSA, 0.1% Tween in PBS). Coverslips were then incubated overnight at 4°C with primary antibodies diluted in antibody dilutant (1% BSA, 0.1% Tween in PBS). Primary antibodies and concentrations are listed in the key resources table. Primary antibodies were washed off with three washes in PBS for 5 min each and then coverslips were incubated for 1 h at room temperature in the dark with Alexa Fluor or Alexa Fluor Plus conjugated secondary antibodies (Thermo Fisher Scientific, Waltham, MA) at a 1:500 dilution in antibody dilutant. Secondary antibodies were washed off with three washes in PBS for 5 min each in the dark. When necessary, coverslips were incubated a second time with fluorescently conjugated β-III-tubulin antibodies (#801203, 1:500, BioLegend, San Diego, CA) for 1 h at room temperature in the dark, then washed three times for 5 min in PBS. After washing, coverslips were dipped in ddH_2O, allowed to briefly air dry in the dark, then mounted with ProLong Diamond Antifade Mountant with or without DAPI (Thermo Fisher Scientific, Waltham, MA) and allowed to cure overnight in the dark.

For synaptic marker and dendritic spine staining, imaging was performed using a Plan-Apochromat 63x/1.4 oil objective on an LSM 800 Axio Observer.Z1 confocal microscope (Zeiss, Thornwood, NY). Images were acquired at 512 × 512 pixels. For each image, a z stack of 7 slices was obtained with an interval of 0.19 μm between each slice. For morphological (Sholl) analysis, 1,388 × 1,040 pixel images were obtained using a Plan-Apochromat 20x/0.8 objective on an Axio-Observer.Z1 microscope equipped with an AxioCam MRm Rev.3 camera (Zeiss, Thornwood, NY). A single plane was obtained for each cell for morphology. Imaging settings were kept constant between all images for each replicate. In general, 10 optical fields were obtained per coverslip with a minimum of two coverslips per condition in each replicate.

Synaptic marker quantification—Image acquisition and analysis were performed by an experimenter blind to the experimental condition. During image acquisition, all optical fields were chosen to contain a single neuronal soma in the center of the field with surrounding neurites. Images in CZI format were imported into Fiji[63] using Bio-Formats Importer plugin.[80] Maximum intensity projections were created for each channel, and then channels were merged. Merged image was converted to RGB and saved in TIFF format. The channel representing the cell marker (eGFP, ZsGreen1, or β-III-tubulin) was thresholded using the Huang threshold[79] and the area was measured for normalization.

Counting of synaptic puncta (synapsin I, PSD-95, VGAT, VGLUT1, and gephyrin) was performed using the Puncta Analyzer ImageJ plugin according to the author's instructions.[21] Merged TIFF images were opened in ImageJ 1.29[81] using Windows OS. The rectangle tool was used to draw a region of interest (ROI) that encompassed the entire field. The plugin was then initiated and quantification was performed using background subtraction with a rolling ball radius of 50. Thresholds were adjusted for each channel for optimal identification of puncta with minimal background signal. Comparable relative threshold settings based on the intensity histogram were used across all images in the same replicate for each channel. Minimum puncta size of 4 pixels and maximum puncta size of 50–100 pixels was used, depending on the marker being measured. Output values for total number of puncta in each channel and total number of co-localized pre- and post-synaptic puncta

Author Manuscript Author Manuscript Author Manuscript Author Manuscript

were obtained. These numbers were normalized by dividing by the total area of the cell mask obtained previously (average cell area per field ~5,000 μm^2) and multiplying by 100 to obtain the number of puncta per 100 μm^2 cell area. For figures, 2x zoomed insets were made in Fiji using "Zoom in images and stacks" macro by Gilles Carpentier.

Sholl analysis—Image acquisition and analysis were performed by an experimenter blind to the experimental condition. Images in CZI format were imported into Fiji[63] using Bio-Formats Importer plugin.[80] MAP2 channel was isolated. RenyiEntropy threshold was applied[82] to create a binary image, then manually adjusted to obtain maximal coverage of the neuron with minimal background. Analyze particles was performed with a particle size of 100-infinity μm^2 to remove remaining background signal. "Close" was performed under binary processing to smooth edges. The line tool was used to draw a line from the center of the soma to the end of the longest dendrite. The Sholl Analysis plugin[83] was then implemented to measure dendrite complexity using the following parameters: starting radius of 25 μm, radius step size of 2 μm, no hemishells (use full shells), 1 sample per radius. Output (number of crossings per radius) was obtained and plotted. Curves were segmented into sections of 50 μm radius and area under each segment of the curve was calculated. The last segment of the curve encompassed 60 μm.

Dendritic spine analysis—Primary hippocampal neurons were prepared, stained for MAP2, and imaged as described above with the following exceptions: neurons were plated at a lower density (20,000–30,000 cells/well in a 12-well plate), fixed in 1.5% PFA instead of 4% PFA, and the Phalloidin-iFluor 647 reagent was added during the secondary antibody incubation step (Abcam, Waltham, MA). Optical fields were chosen to contain at least one dendritic branch that did not intersect with other dendrites. All images were processed using the Fast Iterative Deconvolution parameter in ZEN Blue. Images were converted to TIFF format as described above and the MAP2 channel was used for quantification due to enhanced signal-to-noise ratio. Briefly, the rectangle tool was used to draw a 20 μm × 10 μm ROI that encompassed a representative dendritic segment with no intersecting dendritic branches. Dendritic protrusions were counted manually using the Cell Counter plugin and the total number of spines per ROI was divided by 20 to obtain the number of protrusions per μm. For spine length measurement, the line tool was used to draw a line from the edge of the dendrite to the tip of the protrusion for each protrusion in the ROI, and the protrusion length in microns was recorded.

Live calcium imaging—Primary rat hippocampal neurons were plated at a density of 40,000 cells/well on 12 mm glass coverslips (thickness 0.13–0.17 mm) (Carolina Biological Supply, Burlington, NC) in 24-well culture plates and cultured for 20 days. On DIV1, cells were infected with lentiviruses expressing shControl-mLumin or shPum-mLumin. On DIV15, cells were infected with AAV1-syn-jGCaMP8f[61] (#162376-AAV1, Addgene, Watertown, MA) at a 1:10,000 dilution (final dose ~2×10^9 GC ml^{-1}). AAV1-*syn*-jGCaMP8f was a generous gift from the Janelia Genetically Encoded Neuronal Indicators and Effectors (GENIE) project. FdU/U was not added to the culture past DIV10. On DIV20, coverslips were removed and placed on microscope stage in perfusion imaging setup pre-filled with calcium imaging buffer (130 mM NaCl, 3 mM KCl, 2.5 mM $CaCl_2$,

Author Manuscript Author Manuscript Author Manuscript Author Manuscript

0.6 mM $MgCl_2$, 10 mM HEPES, 1.2 mM $NaHCO_3$, 10 mM glucose, 21 mM sucrose, adjusted to 290–300 mOsm). The microscope stage was pre-heated to 37°C and maintained at 5% CO_2 using a Tokai Hit stage-top incubator with internal humidifier bath (Tokai Hit, Shizuoka, Japan). After placing coverslip, approximately 2 mL fresh calcium imaging buffer was perfused over the coverslip at a rate of approximately 1 mL min^{-1} using SmartSquirt Micro-Perfusion System (AutoMate Scientific, Berkeley, CA) at 30 psi. Perfusion system was then turned off and cells were allowed to equilibrate in buffer for 2 min prior to imaging.

Videos were acquired at 10 Hz with a 2,048 × 2,048 pixel region of interest using Apo LWD 40x/1.15 water immersion objective with a pinhole size of 50 μm on Nikon Eclipse Ti2 inverted microscope (Nikon Instruments Inc., Melville, NY) equipped with Yokogawa spinning disk confocal scanner unit W-1 (Yokogawa Test & Measurement Corporation, Tokyo, Japan) and ORCA-Fusion BT digital camera (Hamamatsu Photonics, Shizuoka, Japan). Fields were selected that contained approximately 5–10 neurons expressing both GCaMP8f and mLumin and in which GCaMP8f signal was not saturated. Emission of green fluorescence was detected resulting from excitation using 488 nm laser at 15% power. Fresh calcium imaging buffer was constantly perfused over cells during imaging session at a rate of approximately 1 mL min^{-1}. After 3 min of video acquisition, 100 mM KCl in calcium imaging buffer was perfused over the cells for 45 s to observe proper calcium response as an indicator of cell health. KCl was washed out with calcium imaging buffer for 1 min and then recording was stopped. Only one field was acquired per coverslip because high KCl concentrations are toxic to cells.

For analysis, videos in AVI format were imported into Fiji[63] using Bio-Formats Importer plugin.[80] ROIs were drawn manually using the selection tool around every neuronal soma. Neurons were excluded if they did not have any visible response to KCl treatment. Three circular selections of equal size were made in background regions of the video which were confirmed to have no neurites present. Raw fluorescence over time for each ROI was extracted using the Time Series Analyzer plugin. Background ROI intensities were averaged for each video and subtracted from somatic ROIs at each time point.

All following analyses were done using custom a MATLAB script. First, raw fluorescence traces were de-trended and normalized ($F - F_0/F_0$). This resulting signal, ΔF/F, was used for all further Ca^{2+} analyses. To calculate single-cell frequency and amplitude, we first fit a Gaussian curve to each cell's baseline activity (excluding outliers ± 3SD). Significant events were detected if a cell's activity went above a set threshold (±3SD of the fit Gaussian curve), with a minimum distance between events (500 ms). Frequency was calculated as the number of detected events per minute. Amplitude is ΔF/F at the time of event. To calculate the correlation coefficient of each imaging session, we calculated the correlation coefficient between all pairs of cells in the FOV and averaged over all values.

RNA isolation and RT-qPCR—Primary rat hippocampal neurons were plated at a density of 100,000–200,000 cells/well in 12-well plates and cultured for 14 days. Cells were washed twice in 2 mL ice-cold DPBS containing calcium and magnesium (Thermo Fisher Scientific, Waltham, MA) and then lysed in 300 μL TRIzol Reagent (Thermo Fisher Scientific,

Author Manuscript Author Manuscript Author Manuscript Author Manuscript

Waltham, MA), scraped with a cell scraper, and mixed thoroughly with an equal volume of 100% ethanol. Total RNA was isolated using the Direct-zol RNA MicroPrep kit (Zymo Research, Irvine, CA) with DNase I treatment according to manufacturer's instructions, with the following changes: RNA wash buffer step (#7) was repeated a second time, followed by centrifugation of empty column for 2 min at 10,000–16,000 × *g* to fully remove wash buffer. RNA concentration was quantified by NanoDrop. RT-qPCR was performed using Luna Universal Probe One-Step RT-qPCR kit (New England Biolabs, Ipswich, MA) according to manufacturer's instructions using 10 ng template RNA per well with Taqman FAM probes (Thermo Fisher Scientific, Waltham, MA) for detection, listed in the key resources table. A 60-s extension time was used as specified for use in the QuantStudio 3 Real-Time PCR System (Thermo Fisher Scientific, Waltham, MA).

RNA immunoprecipitation—RNA immunoprecipitation (IP) protocol was adapted from previous publications.[84,85] All buffers were prepared in nuclease-free water. Input was one cortex per IP reaction from wild-type Sprague Dawley E17 rat embryos. Cortices were pooled and added to 400 μL polysome lysis buffer (PLB) (10 mM HEPES pH 7, 100 mM KCl, 5 mM $MgCl_2$. 0.5% Tergitol) containing 1 mM DTT, 0.1 U μl^{-1} SUPERase·In RNase Inhibitor (Thermo Fisher Scientific, Waltham, MA), and 1X Halt Protease and Phosphatase Inhibitor Cocktail (Thermo Fisher Scientific, Waltham, MA) added fresh. Cortices were homogenized in PLB using glass Dounce tissue grinder #19 (Kontes, Vineland, NJ) for 30 strokes. Samples were allowed to rest for 5 min on ice, homogenized further using a 21G needle for 20 strokes, and then allowed to rest for 5 min on ice again. Samples were then snap-frozen in liquid nitrogen and stored overnight at −80°C.

The next day, 50 μL of Dynabeads M-280 Sheep Anti-Rabbit IgG (Thermo Fisher Scientific, Waltham, MA) were added to an RNase-free microcentrifuge tube for each IP reaction and washed three times for 5 min each in NT-2 buffer (50 mM Tris-HCl pH 7.4, 150 mM NaCl, 1 mM $MgCl_2$, 0.05% Tergitol). After each wash, a magnetic rack was used to separate the beads. Beads were then blocked for 2 h at 4°C with rotation in 500 μL NT-2 buffer containing 0.5 μg mL^{-1} yeast tRNA. Beads were washed briefly three times in NT-2 buffer then incubated for 2 h at 4°C with rotation with 12 μg primary antibodies in 200 μL NT-2 buffer (Pum1 Bethyl #A302–576A; Pum2 Bethyl #A300–202A; rabbit IgG Cell Signaling #2729). Beads were washed quickly 6 times in NT-2 buffer. Cortical lysates were thawed quickly and centrifuged at 14,000 × *g* for 10 min at 4°C. Supernatant was collected and pellet was discarded. After the final wash was removed from the beads, 100 μL cortical lysate supernatant was added to each reaction with 900 μL NET-2 buffer (NT-2 buffer plus 20 mM EDTA pH 8, 1 mM DTT, 0.1 U μl^{-1} SUPERase·In, and 1X Pierce protease and phosphatase inhibitor tablets (Thermo Fisher Scientific, Waltham, MA)). IP reactions were performed overnight at 4°C with rotation. Remaining lysate was saved for input.

Following overnight IP reaction, beads were washed 6 times for 10 min each in NT-2 buffer containing 0.1 U μl^{-1} SUPERase·In and 1X Pierce protease and phosphatase inhibitors. After last wash, 10% of beads were set aside and mixed with 1x Laemmli buffer (2% SDS, 10% glycerol, 60 mM Tris-HCl pH 6.8, 5% β-Mercaptoethanol added fresh) for Western blot analysis. After fully removing NT-2 buffer from remaining beads, 300 μL TRIzol Reagent (Thermo Fisher Scientific, Waltham, MA) was added and tubes were inverted

Author Manuscript Author Manuscript Author Manuscript Author Manuscript

several times to fully resuspend beads. Tubes were centrifuged for 2 min at 5000 × *g* to pellet beads and sample was moved to a new tube. Equal volume of 100% ethanol was added to samples in TRIzol. RNA was isolated using Direct-zol RNA MicroPrep kit (Zymo Research, Irvine, CA) as described above. RNA yield was quantified by NanoDrop and RT-qPCR was performed as described above.

qRT-PCR quantification—Cycle threshold (CT) values were averaged across triplicates for each sample. Signal was normalized by subtracting the CT values of housekeeping gene *Rps19* from the target CT values to generate a ΔCT value. To obtain ΔΔCT values, the ΔCT of the control condition was subtracted from each sample ΔCT. Fold change was calculated using the formula $2^{-\Delta\Delta CT}$. For graphical representation, fold change ($2^{-\Delta\Delta CT}$) was plotted. For statistical analysis, ΔCT values were compared using a paired t test or repeated measures one-way ANOVA matching values from the same replicate.

For RNA immunoprecipitation of Pum1 and Pum2, IP samples were normalized to input by subtracting input *Snap25* and *Rps19* CT values from corresponding IP CT values. The resulting ΔCT values for *Snap25* and *Rps19* were compared to each other using a paired t test to measure enrichment of *Snap25* over *Rps19*. For graphical representation, *Rps19* ΔCT values were subtracted from *Snap25* ΔCT values to yield ΔΔCT values. Fold change ($2^{-\Delta\Delta CT}$) of *Snap25* over *Rps19* was plotted.

Puromycylation—Primary hippocampal neurons were plated on 30 mm glass-bottom optical dishes (MatTek, Ashland, MA) at a density of 125,000 cells per dish. On DIV15, medium was removed from neurons and immediately replaced with 2 mL fresh growth medium containing puromycin at a concentration of 1.84 μM (Thermo Fisher Scientific, Waltham, MA). Cells were incubated for 10 min at 37°C, washed twice quickly with warm DPBS containing calcium and magnesium (Thermo Fisher Scientific, Waltham, MA), and fixed with 4% paraformaldehyde in cytoskeletal preservation buffer as described above. Fixed cells were immediately processed or stored briefly at 4°C before processing. For anisomycin control experiments, the above protocol was preceded by briefly removing and pooling the neuronal culture medium and then replacing 1 mL per dish of this conditioned medium to ensure equivalent volumes across all dishes. Anisomycin and DMSO vehicle dilutions were prepared in fresh growth medium and 1 mL was added to each dish for a final concentration of 40 μM anisomycin or 0.05% DMSO. Cells were incubated for 30 min at 37°C. Puromycin stock (18.4 mM) was diluted 1:100 in fresh growth medium, then 20 μL was added to each plate containing 2 mL medium with anisomycin or DMSO (final dilution 1:10,000; final concentration 1.84 μM). Cells were incubated 10 more minutes at 37°C, then washed and fixed as described above.

Puromycin labeling coupled with proximity ligation assay—Puromycin labeling coupled with proximity ligation assay (puro-PLA) for the detection of newly synthesized proteins was performed according to an established protocol.[32] Following puromycylation and fixation as described above, cells were washed three times for 5 min with PBS containing 100 mM glycine, then permeabilized for 5 min in 0.3% Triton X-100 in PBS. Triton X-100 was removed with two brief washes in PBS, then coverslips were incubated for 30 min at room temperature in blocking buffer (1% BSA, 0.1% Tween in PBS). Samples

Author Manuscript Author Manuscript Author Manuscript Author Manuscript

were then incubated overnight at 4°C with primary antibodies against puromycin and SNAP-25 (puromycin: Millipore Sigma #MABE343, 1:1000; SNAP-25: Millipore Sigma #S9684, 1:500). Proximity ligation assay was then carried out using the Duolink *in situ* assay (Millipore Sigma, St. Louis, MO) according to the manufacturer's instructions. Primary antibodies were washed off with wash buffer A (0.15 M NaCl, 0.01 M Tris, 0.05% Tween, pH 7.4) (3 washes, 5 min each). PLA probes were diluted 1:5 in blocking buffer and incubated for 20 min at room temperature. Probes used were Duolink *in situ* PLA anti-mouse PLUS with anti-rabbit MINUS, or anti-mouse MINUS with anti-rabbit PLUS (Millipore Sigma, St. Louis, MO). Diluted probes were applied to samples and incubated for 1 h at 37°C in a humidity chamber. Probes were washed off with wash buffer A (2 washes, 5 min each) and samples were incubated with ligase at a 1:40 dilution in ligation stock for 30 min at 37°C in a humidity chamber. Ligase solution was washed off with wash buffer A (2 washes, 2 min each) and samples were incubated with polymerase diluted 1:80 in amplification stock (Duolink *in situ* red or far-red detection reagents, Millipore Sigma, St. Louis, MO) for 1 h 40 min at 37°C in a humidity chamber in the dark. Samples were washed with wash buffer B (0.1 M NaCl, 0.2 M Tris, pH 7.5) (2 washes, 10 min each, in the dark), followed by one wash for 1 min with 0.01x wash buffer B. Samples were incubated for 1 h at room temperature in the dark with fluorescently conjugated β-III-tubulin antibody (#801203, 1:500, BioLegend, San Diego, CA) diluted in 0.01x wash buffer B. Samples were washed in 0.01x wash buffer B (3 washes, 5 min each, in the dark), allowed to briefly air dry in the dark, and coverslips were mounted with Duolink *In Situ* mounting medium with DAPI (Millipore Sigma, St. Louis, MO). Mounting medium was allowed to sit for 15 min at room temperature, and samples were then immediately imaged using a Plan-Apochromat 40x/1.3 oil immersion objective on an LSM 800 Axio Observer.Z1 confocal microscope (Zeiss, Thornwood, NY). Approximately 7 fields at 512 × 512 pixels were obtained per optical dish with 2–3 optical dishes per condition in each replicate. For each image, a z stack of 4 slices was obtained with an interval of 0.4 μm between each slice.

PLA quantification—During image acquisition, all optical fields were chosen to contain a single neuronal soma in the center of the field with surrounding neurites. Images in CZI format were imported into Fiji[63] using Bio-Formats Importer plugin.[80] Maximum intensity projections were created for each channel. The channel containing the cell marker (eGFP or β-III-tubulin) was thresholded using Huang2[79] or Mean threshold,[86] and the total cell area was measured for normalization. The channel containing the PLA signal was thresholded using Moments[87] or MaxEntropy.[82] The same thresholds were applied to all images in each replicate. Puncta were then counted using the Analyze Particles function with a particle size of 0.2–5 μm. Puncta count was normalized by dividing by the total area of the cell mask and multiplying by 100 to obtain the number of puncta per 100 μm^2 cell area. To produce neurite-specific counts, an ROI was manually drawn around the cell soma and analysis was repeated with the ROI excluded.

QUANTIFICATION AND STATISTICAL ANALYSIS

Statistical analysis—All statistical analyses for *in vitro* experiments were performed using GraphPad Prism 9 (version 9.4.0) (GraphPad Software, San Diego, CA). Most statistical tests used were non-parametric to eliminate potential outlier effects and avoid

Author Manuscript Author Manuscript Author Manuscript Author Manuscript

making assumptions about the distribution of the data points. Unless otherwise specified, comparison of two groups was performed using the Mann-Whitney test. Comparison of three or more groups was performed using the Kruskal-Wallis test with uncorrected Dunn's test (for a small number of comparisons to the same control sample). In cases where the sample size was insufficient for a nonparametric test, an unpaired t test was used for comparison of two groups and one-way ANOVA for comparison of two or more groups. For evaluating the effect of two independent variables, a two-way ANOVA with Šidák's multiple comparisons test was performed. Specific details on statistical tests used and sample size for each experiment can be found in the figure legends. For statistical analysis, experiments were performed on 3–5 biological replicates (independent cultures), with 10–20 samples from each biological replicate for imaging studies.

Sequencing data acquisition and access—iCLIP data for Pum1 and Pum2 in mouse brains, formatted as BED files, were acquired from the GEO database (GEO accession number GSE95195).[18] Additionally, raw RNA sequencing FASTQ files for Pum1, Pum2, and their double knockdown are available under GEO accession number GSE95102.[18] RNA sequencing data for the developing mouse cortex was obtained from the SRA database (SRA accession number PRJNA275412).[20]

iCLIP target analysis—The BED files from two biological replicates of iCLIP experiments, which contain peaks representing significantly bound genomic regions by Pum1 and Pum2 in wild-type mouse brains, were processed using Bedtools (v2.30.0)[64] and the mm10 UCSC annotation to extract genes significantly bound by either Pum1 or Pum2. Only genes present in both replicates were used for downstream analysis. Gene ontology analysis for Pum1 and Pum2 targets was performed with clusterProfiler (v4.10.0)[66,67] and SynGO (v1.2).[29] For clusterProfiler gene annotations were obtained from AnnotationDbi[71] and org.Mm.e.g.,.db.[72] For SynGO settings, brain-expressed genes were used as background. A full description of SynGO categories displayed and the genes included in each category can be found at https://www.syngoportal.org/ontology.

Transcriptome expression analysis—FASTQ file reads were pseudoaligned using Salmon (v1.10.1)[65] against the GRCm39 gencode v34 mouse transcriptome, with the GRCm39 mouse genome as a decoy. Transcript quantifications by Salmon were imported in R using tximport (v1.30.0)[68] and differential gene expression analysis was performed with Limma-Voom (v3.58.1).[69,70] Only genes with more than 20 reads per condition were used for downstream analysis. Gene set enrichment analysis was performed in the log2 fold change ranked list using ClusterProfiler. Only categories related to synaptic development, axon growth, translation regulation, and mitochondrial function are shown. Data processing in R was performed using the dplyr[73] and tidyr[74] packages. Heatmaps, data visualization, and figures were created using the pheatmap[75] and ggplot2[76] packages.

Supplementary Material

Refer to Web version on PubMed Central for supplementary material.

Author Manuscript Author Manuscript Author Manuscript Author Manuscript

ACKNOWLEDGMENTS

This research was supported by the National Institutes of Neurological Disorders and Stroke and of Cancer of the NIH under the following award numbers: L.K.R.: F31NS113574, T32NS064928, and T32NS115699; L.J.S.: F31NS11 1853; and J.C.M.: T32CA244125, T32CA285257, and 2K12CA120780–16. U.H. was supported by a Taub Institute Grant for Emerging Research. K.V.R. was supported through the NIH Director's Early Independence Award, DP5OD028133, and by the Fidelity Biomedical Research Initiative. The authors thank Nadia Fazel for assistance with image acquisition for Sholl experiments. The graphical abstract was created with BioRender.com.

REFERENCES

1. Xing L, and Bassell GJ (2013). mRNA localization: an orchestration of assembly, traffic and synthesis. Traffic 14, 2–14. 10.1111/tra.12004. [PubMed: 22913533]
2. Corbett AH (2018). Post-transcriptional regulation of gene expression and human disease. Curr. Opin. Cell Biol. 52, 96–104. 10.1016/j.ceb.2018.02.011. [PubMed: 29518673]
3. Krug M, Lö ssner B, and Ott T (1984). Anisomycin blocks the late phase of long-term potentiation in the dentate gyrus of freely moving rats. Brain Res. Bull. 13, 39–42. 10.1016/0361-9230(84)90005-4. [PubMed: 6089972]
4. Montarolo PG, Goelet P, Castellucci VF, Morgan J, Kandel ER, and Schacher S (1986). A critical period for macromolecular synthesis in long-term heterosynaptic facilitation in Aplysia. Science 234, 1249–1254. 10.1126/science.3775383. [PubMed: 3775383]
5. Otani S, Marshall CJ, Tate WP, Goddard GV, and Abraham WC (1989). Maintenance of long-term potentiation in rat dentate gyrus requires protein synthesis but not messenger RNA synthesis immediately post-tetanization. Neuroscience 28, 519–526. 10.1016/0306-4522(89)90001-8. [PubMed: 2710327]
6. Kang H, and Schuman EM (1996). A requirement for local protein synthesis in neurotrophin-induced hippocampal synaptic plasticity. Science 273, 1402–1406. 10.1126/science.273.5280.1402. [PubMed: 8703078]
7. Ouyang Y, Rosenstein A, Kreiman G, Schuman EM, and Kennedy MB (1999). Tetanic stimulation leads to increased accumulation of Ca(2+)/calmodulin-dependent protein kinase II via dendritic protein synthesis in hippocampal neurons. J. Neurosci. 19, 7823–7833. 10.1523/JNEUROSCI.19-18-07823.1999. [PubMed: 10479685]
8. Miller S, Yasuda M, Coats JK, Jones Y, Martone ME, and Mayford M (2002). Disruption of dendritic translation of CaMKIIalpha impairs stabilization of synaptic plasticity and memory consolidation. Neuron 36, 507–519. 10.1016/s0896-6273(02)00978-9. [PubMed: 12408852]
9. Steward O, Wallace CS, Lyford GL, and Worley PF (1998). Synaptic activation causes the mRNA for the IEG Arc to localize selectively near activated postsynaptic sites on dendrites. Neuron 21, 741–751. 10.1016/s0896-6273(00)80591-7. [PubMed: 9808461]
10. Steward O, and Worley PF (2001). Selective targeting of newly synthesized Arc mRNA to active synapses requires NMDA receptor activation. Neuron 30, 227–240. 10.1016/s0896-6273(01)00275-6. [PubMed: 11343657]
11. Yin Y, Edelman GM, and Vanderklish PW (2002). The brain-derived neurotrophic factor enhances synthesis of Arc in synaptoneurosomes. Proc. Natl. Acad. Sci. USA 99, 2368–2373. 10.1073/pnas.042693699. [PubMed: 11842217]
12. Ying SW, Futter M, Rosenblum K, Webber MJ, Hunt SP, Bliss TVP, and Bramham CR (2002). Brain-derived neurotrophic factor induces long-term potentiation in intact adult hippocampus: requirement for ERK activation coupled to CREB and upregulation of Arc synthesis. J. Neurosci. 22, 1532–1540. 10.1523/JNEUROSCI.22-05-01532.2002. [PubMed: 11880483]
13. An JJ, Gharami K, Liao GY, Woo NH, Lau AG, Vanevski F, Torre ER, Jones KR, Feng Y, Lu B, and Xu B (2008). Distinct role of long 3' UTR BDNF mRNA in spine morphology and synaptic plasticity in hippocampal neurons. Cell 134, 175–187. 10.1016/j.cell.2008.05.045. [PubMed: 18614020]
14. Younts TJ, Monday HR, Dudok B, Klein ME, Jordan BA, Katona I, and Castillo PE (2016). Presynaptic Protein Synthesis Is Required for Long-Term Plasticity of GABA Release. Neuron 92, 479–492. 10.1016/j.neuron.2016.09.040. [PubMed: 27764673]

Author Manuscript Author Manuscript Author Manuscript Author Manuscript

15. Taylor AM, Wu J, Tai HC, and Schuman EM (2013). Axonal translation of beta-catenin regulates synaptic vesicle dynamics. J. Neurosci. 33, 5584–5589. 10.1523/JNEUROSCI.2944-12.2013. [PubMed: 23536073]
16. Batista AFR, Martínez JC, and Hengst U (2017). Intra-axonal Synthesis of SNAP25 Is Required for the Formation of Presynaptic Terminals. Cell Rep. 20, 3085–3098. 10.1016/j.celrep.2017.08.097. [PubMed: 28954226]
17. Martínez JC, Randolph LK, Iascone DM, Pernice HF, Polleux F, and Hengst U (2019). Pum2 Shapes the Transcriptome in Developing Axons through Retention of Target mRNAs in the Cell Body. Neuron 104, 931–946.e935. 10.1016/j.neuron.2019.08.035. [PubMed: 31606248]
18. Zhang M, Chen D, Xia J, Han W, Cui X, Neuenkirchen N, Hermes G, Sestan N, and Lin H (2017). Post-transcriptional regulation of mouse neurogenesis by Pumilio proteins. Genes Dev. 31, 1354–1369. 10.1101/gad.298752.117. [PubMed: 28794184]
19. Arey RN, Kaletsky R, and Murphy CT (2019). Nervous system-wide profiling of presynaptic mRNAs reveals regulators of associative memory. Sci. Rep. 9, 20314. 10.1038/s41598-019-56908-8. [PubMed: 31889133]
20. Weyn-Vanhentenryck SM, Feng H, Ustianenko D, Duffié R, Yan Q, Jacko M, Martinez JC, Goodwin M, Zhang X, Hengst U, et al. (2018). Precise temporal regulation of alternative splicing during neural development. Nat. Commun. 9, 2189. 10.1038/s41467-018-04559-0. [PubMed: 29875359]
21. Ippolito DM, and Eroglu C (2010). Quantifying synapses: an immunocy-tochemistry-based assay to quantify synapse number. J. Vis. Exp. 10, 2270.
22. Verstraelen P, Garcia-Diaz Barriga G, Verschuuren M, Asselbergh B, Nuydens R, Larsen PH, Timmermans JP, and De Vos WH (2020). Systematic Quantification of Synapses in Primary Neuronal Culture. iScience 23, 101542. 10.1016/j.isci.2020.101542. [PubMed: 33083769]
23. Fiore R, Rajman M, Schwale C, Bicker S, Antoniou A, Bruehl C, Draguhn A, and Schratt G (2014). MiR-134-dependent regulation of Pumilio-2 is necessary for homeostatic synaptic depression. EMBO J. 33, 2231–2246. 10.15252/embj.201487921. [PubMed: 25097251]
24. Vessey JP, Schoderboeck L, Gingl E, Luzi E, Riefler J, Di Leva F, Karra D, Thomas S, Kiebler MA, and Macchi P (2010). Mammalian Pumilio 2 regulates dendrite morphogenesis and synaptic function. Proc. Natl. Acad. Sci. USA 107, 3222–3227. 10.1073/pnas.0907128107. [PubMed: 20133610]
25. Vessey JP, Vaccani A, Xie Y, Dahm R, Karra D, Kiebler MA, and Macchi P (2006). Dendritic localization of the translational repressor Pumilio 2 and its contribution to dendritic stress granules. J. Neurosci. 26, 6496–6508. 10.1523/JNEUROSCI.0649-06.2006. [PubMed: 16775137]
26. Sholl DA (1953). Dendritic organization in the neurons of the visual and motor cortices of the cat. J. Anat. 87, 387–406. [PubMed: 13117757]
27. Zhang W, and Benson DL (2001). Stages of synapse development defined by dependence on F-actin. J. Neurosci. 21, 5169–5181. 10.1523/JNEUROSCI.21-14-05169.2001. [PubMed: 11438592]
28. Vlachos A, Reddy-Alla S, Papadopoulos T, Deller T, and Betz H (2013). Homeostatic regulation of gephyrin scaffolds and synaptic strength at mature hippocampal GABAergic postsynapses. Cereb. Cortex 23, 2700–2711. 10.1093/cercor/bhs260. [PubMed: 22918984]
29. Koopmans F, van Nierop P, Andres-Alonso M, Byrnes A, Cijsouw T, Coba MP, Cornelisse LN, Farrell RJ, Goldschmidt HL, Howrigan DP, et al. (2019). SynGO: An Evidence-Based, Expert-Curated Knowledge Base for the Synapse. Neuron 103, 217–234.e4. 10.1016/j.neuron.2019.05.002. [PubMed: 31171447]
30. Schieweck R, Riedemann T, Forné I, Harner M, Bauer KE, Rieger D, Ang FY, Hutten S, Demleitner AF, Popper B, et al. (2021). Pumilio2 and Staufen2 selectively balance the synaptic proteome. Cell Rep. 35, 109279. 10.1016/j.celrep.2021.109279. [PubMed: 34161769]
31. Yamada T, Imamachi N, Imamura K, Taniue K, Kawamura T, Suzuki Y, Nagahama M, and Akimitsu N (2020). Systematic Analysis of Targets of Pumilio-Mediated mRNA Decay Reveals that PUM1 Repression by DNA Damage Activates Translesion Synthesis. Cell Rep. 31, 107542. 10.1016/j.celrep.2020.107542. [PubMed: 32375027]

Author Manuscript Author Manuscript Author Manuscript Author Manuscript

32. tom Dieck S, Kochen L, Hanus C, Heumüller M, Bartnik I, Nassim-Assir B, Merk K, Mosler T, Garg S, Bunse S, et al. (2015). Direct visualization of newly synthesized target proteins in situ. Nat. Methods 12, 411–414. 10.1038/nmeth.3319. [PubMed: 25775042]
33. Muraro NI, Weston AJ, Gerber AP, Luschnig S, Moffat KG, and Baines RA (2008). Pumilio binds para mRNA and requires Nanos and Brat to regulate sodium current in Drosophila motoneurons. J. Neurosci. 28, 2099–2109. 10.1523/JNEUROSCI.5092-07.2008. [PubMed: 18305244]
34. Botta S, de Prisco N, Chemiakine A, Brandt V, Cabaj M, Patel P, Doron-Mandel E, Treadway CJ, Jovanovic M, Brown NG, et al. (2023). Dosage sensitivity to Pumilio1 variants in the mouse brain reflects distinct molecular mechanisms. EMBO J. 42, e112721. 10.15252/embj.2022112721. [PubMed: 37070548]
35. Menon KP, Sanyal S, Habara Y, Sanchez R, Wharton RP, Ramaswami M, and Zinn K (2004). The translational repressor Pumilio regulates presynaptic morphology and controls postsynaptic accumulation of translation factor eIF-4E. Neuron 44, 663–676. 10.1016/j.neuron.2004.10.028. [PubMed: 15541314]
36. Driscoll HE, Muraro NI, He M, and Baines RA (2013). Pumilio-2 regulates translation of Nav1.6 to mediate homeostasis of membrane excitability. J. Neurosci. 33, 9644–9654. 10.1523/JNEUROSCI.0921-13.2013. [PubMed: 23739961]
37. Follwaczny P, Schieweck R, Riedemann T, Demleitner A, Straub T, Klemm AH, Bilban M, Sutor B, Popper B, and Kiebler MA (2017). Pumilio2-deficient mice show a predisposition for epilepsy. Dis. Model. Mech. 10, 1333–1342. 10.1242/dmm.029678. [PubMed: 29046322]
38. Siemen H, Colas D, Heller HC, Brüstle O, and Pera RAR (2011). Pumilio-2 function in the mouse nervous system. PLoS One 6, e25932. 10.1371/journal.pone.0025932. [PubMed: 22016787]
39. Wu XL, Huang H, Huang YY, Yuan JX, Zhou X, and Chen YM (2015). Reduced Pumilio-2 expression in patients with temporal lobe epilepsy and in the lithium-pilocarpine induced epilepsy rat model. Epilepsy Behav. 50, 31–39. 10.1016/j.yebeh.2015.05.017. [PubMed: 26101106]
40. Pique M, Lopez JM, Foissac S, Guigo R, and Mendez R (2008). A combinatorial code for CPE-mediated translational control. Cell 132, 434–448. 10.1016/j.cell.2007.12.038. [PubMed: 18267074]
41. Cao Q, Padmanabhan K, and Richter JD (2010). Pumilio 2 controls translation by competing with eIF4E for 7-methyl guanosine cap recognition. RNA 16, 221–227. 10.1261/rna.1884610. [PubMed: 19933321]
42. Goldstrohm AC, Hook BA, Seay DJ, and Wickens M (2006). PUF proteins bind Pop2p to regulate messenger RNAs. Nat. Struct. Mol. Biol. 13, 533–539. 10.1038/nsmb1100. [PubMed: 16715093]
43. Weidmann CA, Raynard NA, Blewett NH, Van Etten J, and Goldstrohm AC (2014). The RNA binding domain of Pumilio antagonizes poly-adenosine binding protein and accelerates deadenylation. RNA 20, 1298–1319. 10.1261/rna.046029.114. [PubMed: 24942623]
44. Van Etten J, Schagat TL, Hrit J, Weidmann CA, Brumbaugh J, Coon JJ, and Goldstrohm AC (2012). Human Pumilio proteins recruit multiple deadenylases to efficiently repress messenger RNAs. J. Biol. Chem. 287, 36370–36383. 10.1074/jbc.M112.373522. [PubMed: 22955276]
45. Blewett NH, and Goldstrohm AC (2012). A eukaryotic translation initiation factor 4E-binding protein promotes mRNA decapping and is required for PUF repression. Mol. Cell Biol. 32, 4181–4194. 10.1128/MCB.00483-12. [PubMed: 22890846]
46. Bohn JA, Van Etten JL, Schagat TL, Bowman BM, McEachin RC, Freddolino PL, and Goldstrohm AC (2018). Identification of diverse target RNAs that are functionally regulated by human Pumilio proteins. Nucleic Acids Res. 46, 362–386. 10.1093/nar/gkx1120. [PubMed: 29165587]
47. Kaye JA, Rose NC, Goldsworthy B, Goga A, and L'Etoile ND (2009). A 3'UTR pumilio-binding element directs translational activation in olfactory sensory neurons. Neuron 61, 57–70. 10.1016/j.neuron.2008.11.012. [PubMed: 19146813]
48. Lehmann R, and Nüsslein-Volhard C (1987). Involvement of the Pumilio Gene in the Transport of an Abdominal Signal in the Drosophila Embryo. Nature 329, 167–170. 10.1038/329167a0.
49. Murata Y, and Wharton RP (1995). Binding of pumilio to maternal hunchback mRNA is required for posterior patterning in Drosophila embryos. Cell 80, 747–756. 10.1016/0092-8674(95)90353-4. [PubMed: 7889568]

Author Manuscript Author Manuscript Author Manuscript Author Manuscript

50. Quenault T, Lithgow T, and Traven A (2011). PUF proteins: repression, activation and mRNA localization. Trends Cell Biol. 21, 104–112. 10.1016/j.tcb.2010.09.013. [PubMed: 21115348]
51. Devine MJ, and Kittler JT (2018). Mitochondria at the neuronal presynapse in health and disease. Nat. Rev. Neurosci. 19, 63–80. 10.1038/nrn.2017.170.
52. Duarte FV, Ciampi D, and Duarte CB (2023). Mitochondria as central hubs in synaptic modulation. Cell. Mol. Life Sci. 80, 173. 10.1007/s00018-023-04814-8. [PubMed: 37266732]
53. Rangaraju V, Lauterbach M, and Schuman EM (2019). Spatially Stable Mitochondrial Compartments Fuel Local Translation during Plasticity. Cell 176, 73–84.e15. 10.1016/j.cell.2018.12.013. [PubMed: 30612742]
54. Lujan BJ, Singh M, Singh A, and Renden RB (2021). Developmental shift to mitochondrial respiration for energetic support of sustained transmission during maturation at the calyx of Held. J. Neurophysiol. 126, 976–996. 10.1152/jn.00333.2021. [PubMed: 34432991]
55. Darnell JC, Van Driesche SJ, Sarah J, Zhang C, Hung KYS, Mele A, Fraser CE, Stone EF, Chen C, Fak JJ, Chi SW, et al. (2011). FMRP Stalls Ribosomal Translocation on mRNAs Linked to Synaptic Function and Autism. Cell 146, 247–261. 10.1016/j.cell.2011.06.013. [PubMed: 21784246]
56. Buss EW, Corbett NJ, Roberts JG, Ybarra N, Musial TF, Simkin D, Molina-Campos E, Oh KJ, Nielsen LL, Ayala GD, et al. (2021). Cognitive aging is associated with redistribution of synaptic weights in the hippocampus. Proc. Natl. Acad. Sci. USA 118, e1921481118. 10.1073/pnas.1921481118. [PubMed: 33593893]
57. Morrison JH, and Baxter MG (2012). The ageing cortical synapse: hallmarks and implications for cognitive decline. Nat. Rev. Neurosci. 13, 240–250. 10.1038/nrn3200. [PubMed: 22395804]
58. Mostany R, Anstey JE, Crump KL, Maco B, Knott G, and Portera-Cailliau C (2013). Altered synaptic dynamics during normal brain aging. J. Neurosci. 33, 4094–4104. 10.1523/JNEUROSCI.4825-12.2013. [PubMed: 23447617]
59. D'Amico D, Mottis A, Potenza F, Sorrentino V, Li H, Romani M, Lemos V, Schoonjans K, Zamboni N, Knott G, et al. (2019). The RNA-Binding Protein PUM2 Impairs Mitochondrial Dynamics and Mitophagy During Aging. Mol Cell 73, 775–787.e710. 10.1016/j.molcel.2018.11.034. [PubMed: 30642763]
60. Kopp F, Elguindy MM, Yalvac ME, Zhang H, Chen B, Gillett FA, Lee S, Sivakumar S, Yu H, Xie Y, et al. (2019). PUMILIO hyperactivity drives premature aging of Norad-deficient mice. Elife 8, e42650. 10.7554/eLife.42650. [PubMed: 30735131]
61. Zhang Y, Ró zsa M, Liang Y, Bushey D, Wei Z, Zheng J, Reep D, Broussard GJ, Tsang A, Tsegaye G, et al. (2023). Fast and sensitive GCaMP calcium indicators for imaging neural populations. Nature 615, 884–891. 10.1038/s41586-023-05828-9. [PubMed: 36922596]
62. Lois C, Hong EJ, Pease S, Brown EJ, and Baltimore D (2002). Germline transmission and tissue-specific expression of transgenes delivered by lentiviral vectors. Science 295, 868–872. 10.1126/science.1067081. [PubMed: 11786607]
63. Schindelin J, Arganda-Carreras I, Frise E, Kaynig V, Longair M, Pietzsch T, Preibisch S, Rueden C, Saalfeld S, Schmid B, et al. (2012). Fiji: an open-source platform for biological-image analysis. Nat. Methods 9, 676–682. 10.1038/nmeth.2019. [PubMed: 22743772]
64. Quinlan AR, and Hall IM (2010). BEDTools: a flexible suite of utilities for comparing genomic features. Bioinformatics 26, 841–842. 10.1093/bioinformatics/btq033. [PubMed: 20110278]
65. Patro R, Duggal G, Love MI, Irizarry RA, and Kingsford C (2017). Salmon provides fast and bias-aware quantification of transcript expression. Nat. Methods 14, 417–419. 10.1038/nmeth.4197. [PubMed: 28263959]
66. Yu G, Wang LG, Han Y, and He QY (2012). clusterProfiler: an R package for comparing biological themes among gene clusters. OMICS 16, 284–287. 10.1089/omi.2011.0118. [PubMed: 22455463]
67. Wu T, Hu E, Xu S, Chen M, Guo P, Dai Z, Feng T, Zhou L, Tang W, Zhan L, et al. (2021). clusterProfiler 4.0: A universal enrichment tool for interpreting omics data. Innovation 2, 100141. 10.1016/j.xinn.2021.100141. [PubMed: 34557778]
68. Soneson C, Love MI, and Robinson MD (2015). Differential analyses for RNA-seq: transcript-level estimates improve gene-level inferences. F1000Res. 4, 1521. 10.12688/f1000research.7563.2. [PubMed: 26925227]

Author Manuscript Author Manuscript Author Manuscript Author Manuscript

69. Ritchie ME, Phipson B, Wu D, Hu Y, Law CW, Shi W, and Smyth GK (2015). limma powers differential expression analyses for RNA-sequencing and microarray studies. Nucleic Acids Res. 43, e47. 10.1093/nar/gkv007. [PubMed: 25605792]
70. Law CW, Chen Y, Shi W, and Smyth GK (2014). voom: precision weights unlock linear model analysis tools for RNA-seq read counts. Genome Biol. 15, R29. 10.1186/gb-2014-15-2-r29. [PubMed: 24485249]
71. Pagè s H, Carlson M, Falcon S, and Li N (2023). AnnotationDbi: Manipulation of SQLite-based annotations in Bioconductor. https://bioconductor.org/packages/release/bioc/html/AnnotationDbi.html10.18129/b9.bioc.annotationdbi.
72. Carlson M (2023). org.Mm.eg.db: Genome Wide Annotation for Mouse.https://bioconductor.org/packages/release/data/annotation/html/org.Mm.eg.db.html10.18129/B9.bioc.org.Mm.eg.db.
73. Wickham H, François R, Henry L, Müller K, and Vaughan D (2023). dplyr: A Grammar of Data Manipulation. https://cran.r-project.org/web/packages/dplyr/index.html10.32614/CRAN.package.dplyr.
74. Wickham H, Vaughan D, and Girlich M (2024). tidyr: Tidy Messy Data. https://cran.r-project.org/web/packages/tidyr/index.html10.32614/CRAN.package.tidyr.
75. Kolde R (2019). Pheatmap: Pretty Heatmaps. https://cran.r-project.org/web/packages/pheatmap/index.html10.32614/CRAN.package.pheatmap.
76. Wickham H (2016). ggplot2: Elegant Graphics for Data Analysis (Springer). 10.1007/978-3-319-24277-4.
77. Auyeung VC, Ulitsky I, McGeary SE, and Bartel DP (2013). Beyond secondary structure: primary-sequence determinants license pri-miRNA hairpins for processing. Cell 152, 844–858. 10.1016/j.cell.2013.01.031. [PubMed: 23415231]
78. Knott SRV, Maceli A, Erard N, Chang K, Marran K, Zhou X, Gordon A, Demerdash OE, Wagenblast E, Kim S, et al. (2014). A computational algorithm to predict shRNA potency. Mol. Cell 56, 796–807. 10.1016/j.molcel.2014.10.025. [PubMed: 25435137]
79. Huang LK, and Wang MJJ (1995). Image Thresholding by Minimizing the Measures of Fuzziness. Pattern Recogn. 28, 41–51. 10.1016/0031-3203(94)E0043-K.
80. Linkert M, Rueden CT, Allan C, Burel JM, Moore W, Patterson A, Loranger B, Moore J, Neves C, Macdonald D, et al. (2010). Metadata matters: access to image data in the real world. J. Cell Biol. 189, 777–782. 10.1083/jcb.201004104. [PubMed: 20513764]
81. Schneider CA, Rasband WS, and Eliceiri KW (2012). NIH Image to ImageJ: 25 years of image analysis. Nat. Methods 9, 671–675. 10.1038/nmeth.2089. [PubMed: 22930834]
82. Kapur JN, Sahoo PK, and Wong AKC (1985). A New Method for Gray-Level Picture Thresholding Using the Entropy of the Histogram. Comput Vision Graph 29, 273–285. 10.1016/0734-189x(85)90125-2.
83. Ferreira TA, Blackman AV, Oyrer J, Jayabal S, Chung AJ, Watt AJ, Sjöström PJ, and van Meyel DJ (2014). Neuronal morphometry directly from bitmap images. Nat. Methods 11, 982–984. 10.1038/nmeth.3125. [PubMed: 25264773]
84. Jain R, Devine T, George AD, Chittur SV, Baroni TE, Penalva LO, and Tenenbaum SA (2011). RIP-Chip analysis: RNA-Binding Protein Immunoprecipitation-Microarray (Chip) Profiling. Methods Mol. Biol. 703, 247–263. 10.1007/978-1-59745-248-9_17. [PubMed: 21125495]
85. Keene JD, Komisarow JM, and Friedersdorf MB (2006). RIP-Chip: the isolation and identification of mRNAs, microRNAs and protein components of ribonucleoprotein complexes from cell extracts. Nat. Protoc. 1, 302–307. 10.1038/nprot.2006.47. [PubMed: 17406249]
86. Glasbey CA (1993). An Analysis of Histogram-Based Thresholding Algorithms. CVGIP-Graph. Model. Im 55, 532–537. 10.1006/cgip.1993.1040.
87. Tsai W-H (1985). Moment-preserving thresolding: A new approach. Comput. Vis. Graph Image Process 29, 377–393. 10.1016/0734-189x(85)90133-1.

Author Manuscript Author Manuscript Author Manuscript Author Manuscript

Highlights

- Pum1 and Pum2 are developmentally downregulated in the brain
- Loss of Pum1/2 increases excitatory and inhibitory synapse density and synapse maturation
- Loss of Pum1/2 upregulates mRNAs involved in mitochondrial function and synaptic translation

Author Manuscript Author Manuscript Author Manuscript Author Manuscript

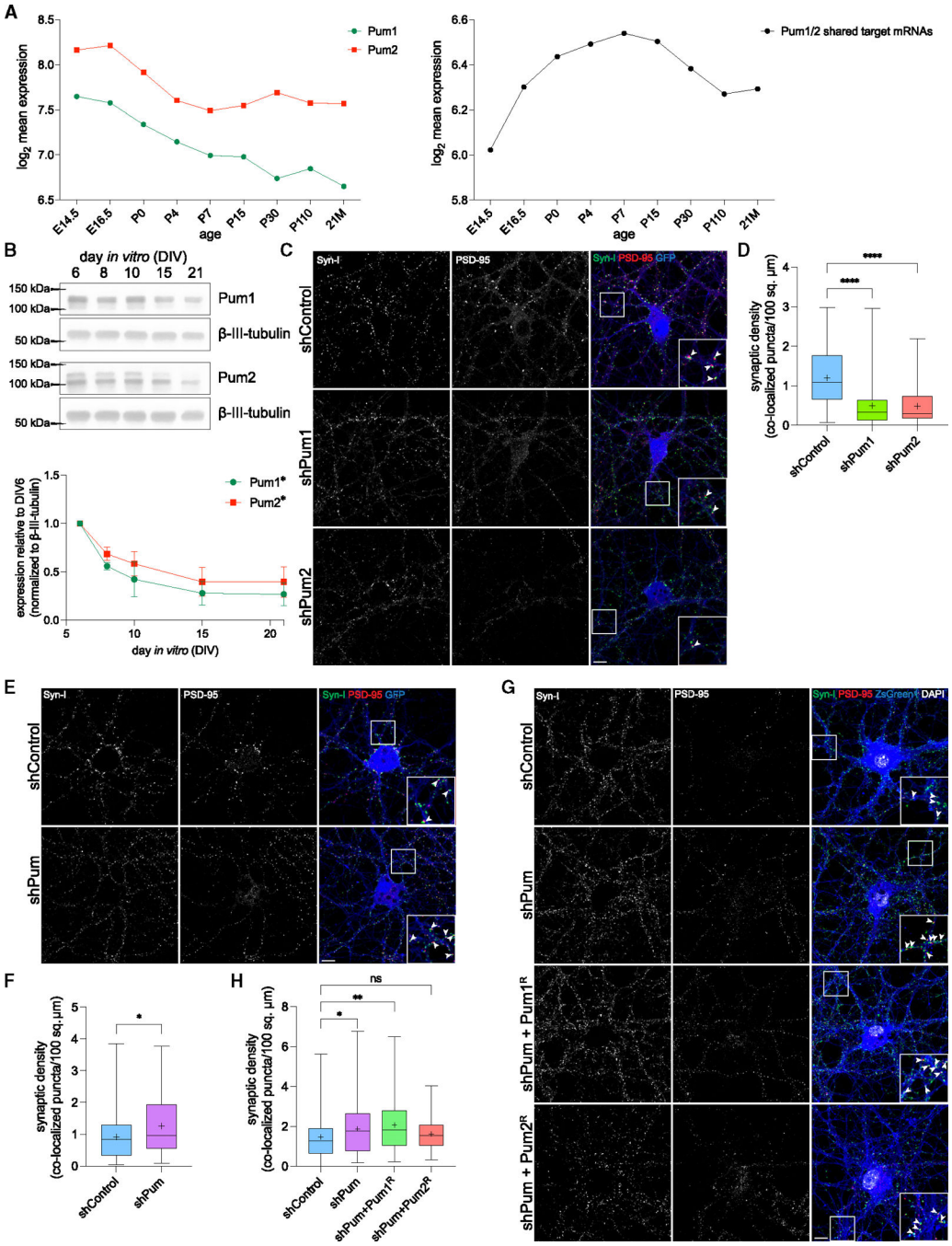

Figure 1. Pumilios regulate synapse density

(A) Developmental mRNA expression of *Pum1* and *Pum2* (left) and their shared mRNA targets (right) in the mouse cortex.

(B) Immunoblotting of Pum1 and Pum2 protein levels in primary rat hippocampal neurons at DIV6–DIV21. Mean ± SEM of $n = 4$ biological replicates. Mixed-effects analysis with Geisser-Greenhouse correction; significance indicator on the protein name indicates an overall fixed effect of DIV on protein level.

Author Manuscript Author Manuscript Author Manuscript Author Manuscript

(C) Neurons infected on DIV2 with shControl, shPum1, or shPum2 lentiviruses were immunostained at DIV14–DIV15 for Syn-I and PSD-95.

(D) Quantification of (C). $n = 80$ fields per condition from 4 biological replicates, Kruskal-Wallis test with uncorrected Dunn's test.

(E) Neurons infected on DIV2 with shControl or shPum lentiviruses were immunostained at DIV14–DIV15 for Syn-I and PSD-95.

(F) Quantification of (E). $n = 59–60$ fields per condition from 3 biological replicates, Mann-Whitney test.

(G) Neurons infected on DIV1 with shControl or shPum lentiviruses and lentiviruses expressing shRNA-resistant Pum1 and Pum2 CDS ($Pum1^R$ and $Pum2^R$) were immunostained at DIV21 for Syn-I and PSD-95.

(H) Quantification of (G). $n = 80$ fields per condition from 4 biological replicates, Kruskal-Wallis test with uncorrected Dunn's test.

(A–H) The total number of co-localized puncta in a field was normalized to the area covered by the cell in the cell marker channel (EGFP or ZsGreen1). Insets, 2× magnification. Arrows indicate co-localized Syn-I+/PSD-95+ puncta. Scale bars, 10 μm. *$p < 0.05$, **$p < 0.01$, ****$p < 0.0001$, and ns, not significant.

Author Manuscript Author Manuscript Author Manuscript Author Manuscript

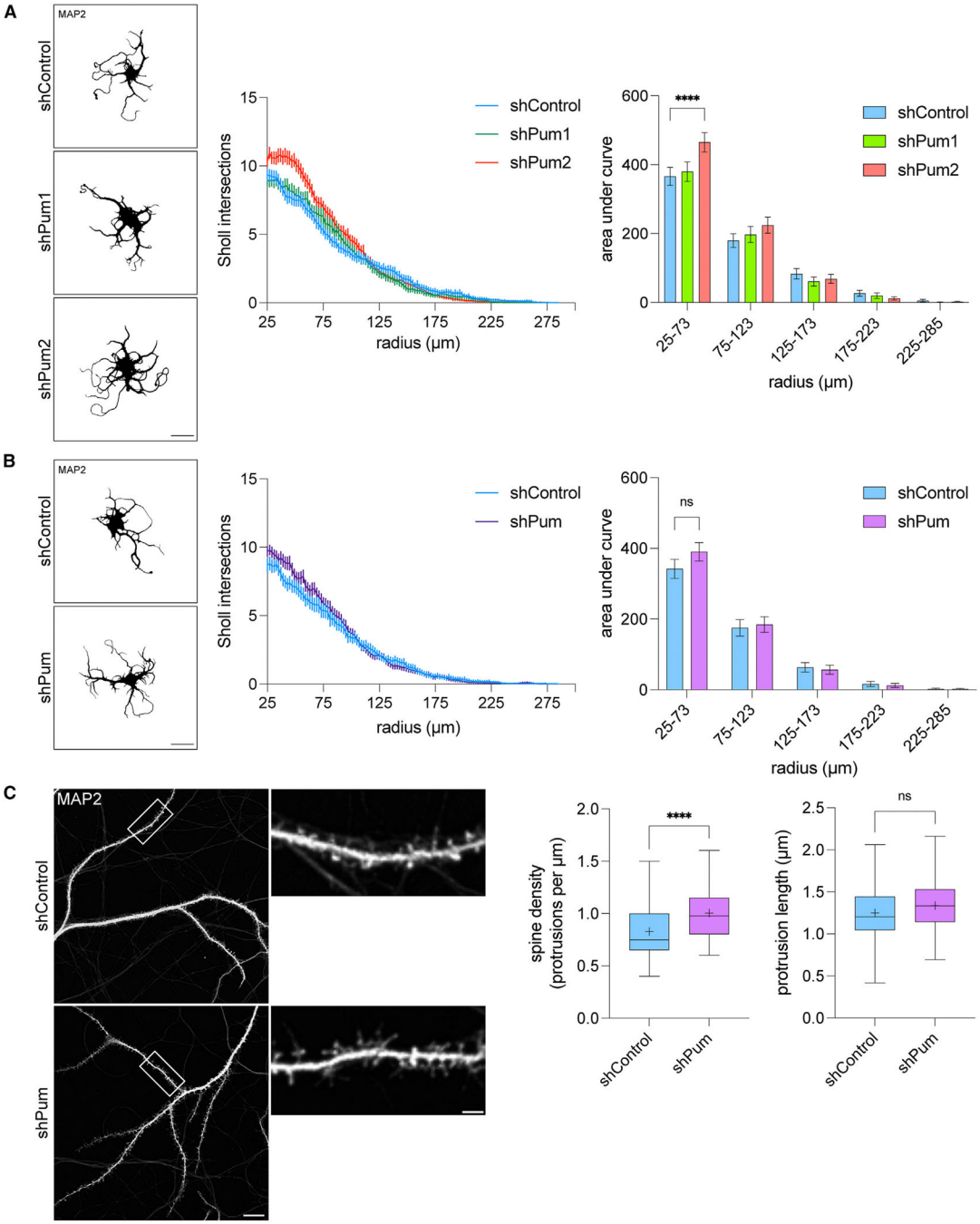

Figure 2. Dual Pumilio downregulation increases spine density but not dendrite complexity

(A) Neurons infected on DIV1 with shControl, shPum1, or shPum2 lentiviruses were immunostained for MAP2 at DIV14. Sholl profiles (left) were segmented into bins of 50 μm for analysis of area under the curve (right). Mean ± SEM of $n = 67–78$ neurons per condition from 4 biological replicates. Two-way ANOVA with Šídák's multiple comparisons test. Scale bars, 50 μm.

Author Manuscript Author Manuscript Author Manuscript Author Manuscript

(B) Neurons infected on DIV1 with shControl or shPum lentiviruses were immunostained for MAP2 at DIV14. Sholl analysis was performed as in (A). Mean ± SEM of n = 70–77 neurons per condition from 4 biological replicates. Scale bars, 50 μm.

(C) Neurons infected on DIV1 with shControl or shPum lentiviruses were immunostained for MAP2 and phalloidin at DIV19, and the MAP2 channel was used for quantification. The density and length of protrusions were measured from regions of interest (ROIs) of single dendrites as pictured. Quantification of $n = 60$ ROIs per condition from 3 biological replicates, Mann-Whitney test. Scale bars, 10 μm in full image and 2 μm in inset.

(A–C) ****$p < 0.0001$ and ns, not significant.

Author Manuscript Author Manuscript Author Manuscript Author Manuscript

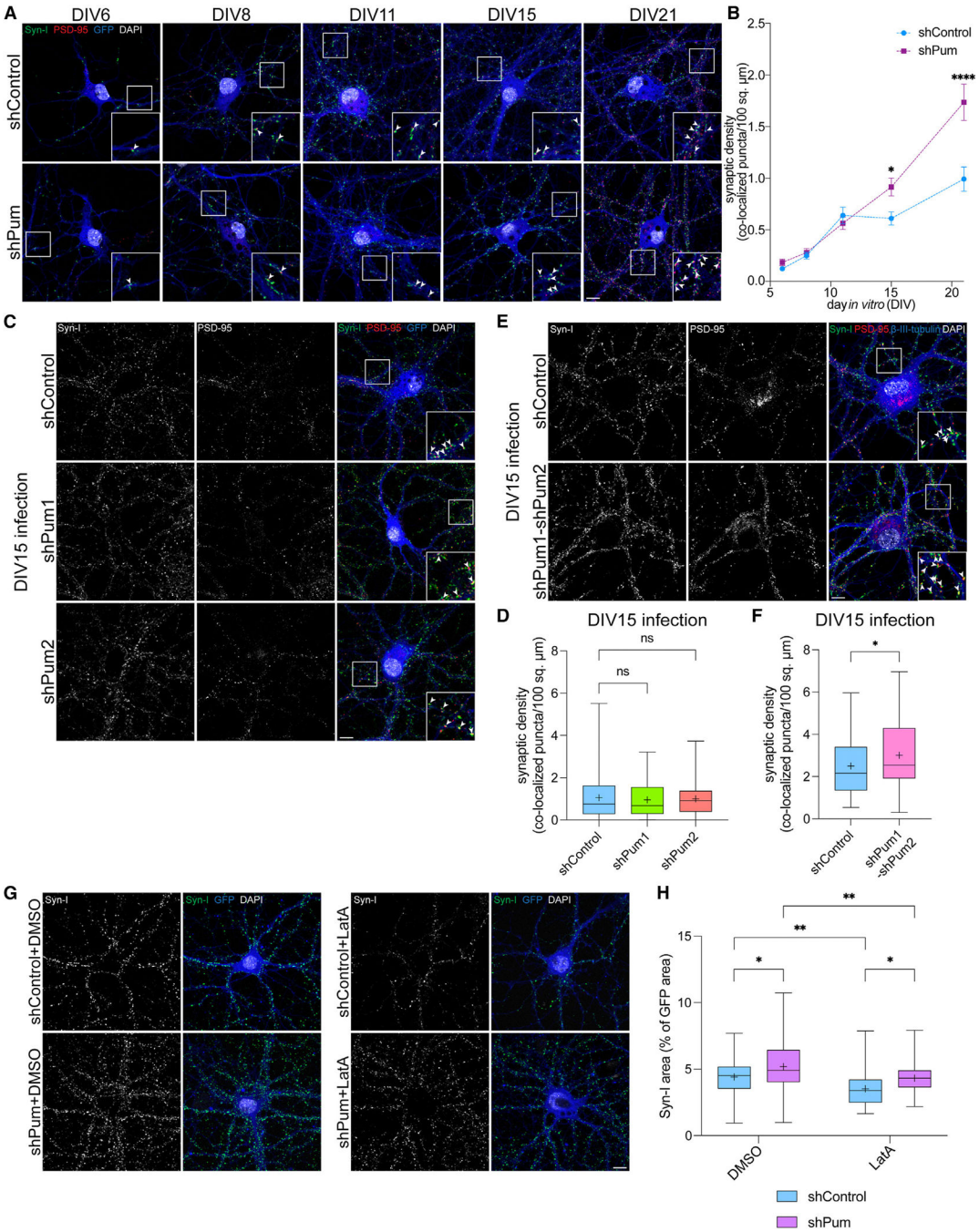

Figure 3. Pumilios regulate synapse density at late stages of maturation by restricting synapse stability

(A) Neurons infected on DIV1 with shControl or shPum lentiviruses were immunostained at DIV6–DIV21 for Syn-I and PSD-95.

(B) Quantification of (A). Two-way ANOVA with Šidák's multiple comparisons test. Mean ± SEM of 56–70 fields per condition/time point from 5 biological replicates.

(C) Neurons infected on DIV15 with shControl, shPum1, or shPum2 lentiviruses were immunostained at DIV21 for Syn-I and PSD-95.

Author Manuscript Author Manuscript Author Manuscript Author Manuscript

(D) Quantification of (C). $n = 100$ optical fields from 5 biological replicates, Kruskal-Wallis test with uncorrected Dunn's test.

(E) Neurons infected on DIV15 with shControl or shPum1-shPum2 lentiviruses were immunostained at DIV21 for Syn-I and PSD-95.

(F) Quantification of (E). $n = 80$ fields from 4 biological replicates, Mann-Whitney test.

(G) Neurons infected on DIV1 with shControl or shPum lentiviruses were treated on DIV18 with 2.5 μM latrunculin A or DMSO and immunostained at DIV19 for Syn-I.

(H) Quantification of (G). n = 59–60 fields from 3 biological replicates, two-way ANOVA with Šidák's multiple comparisons test.

(A–H) The total number of co-localized puncta in a field was normalized to the area covered by the cell in the cell marker channel (EGFP or β-III-tubulin). Inset, 2× magnification. Arrows indicate co-localized Syn-I+/PSD-95+ puncta. Scale bars, 10 μm. *$p < 0.05$, **$p < 0.01$, ****$p < 0.0001$, and ns, not significant.

Author Manuscript Author Manuscript Author Manuscript Author Manuscript

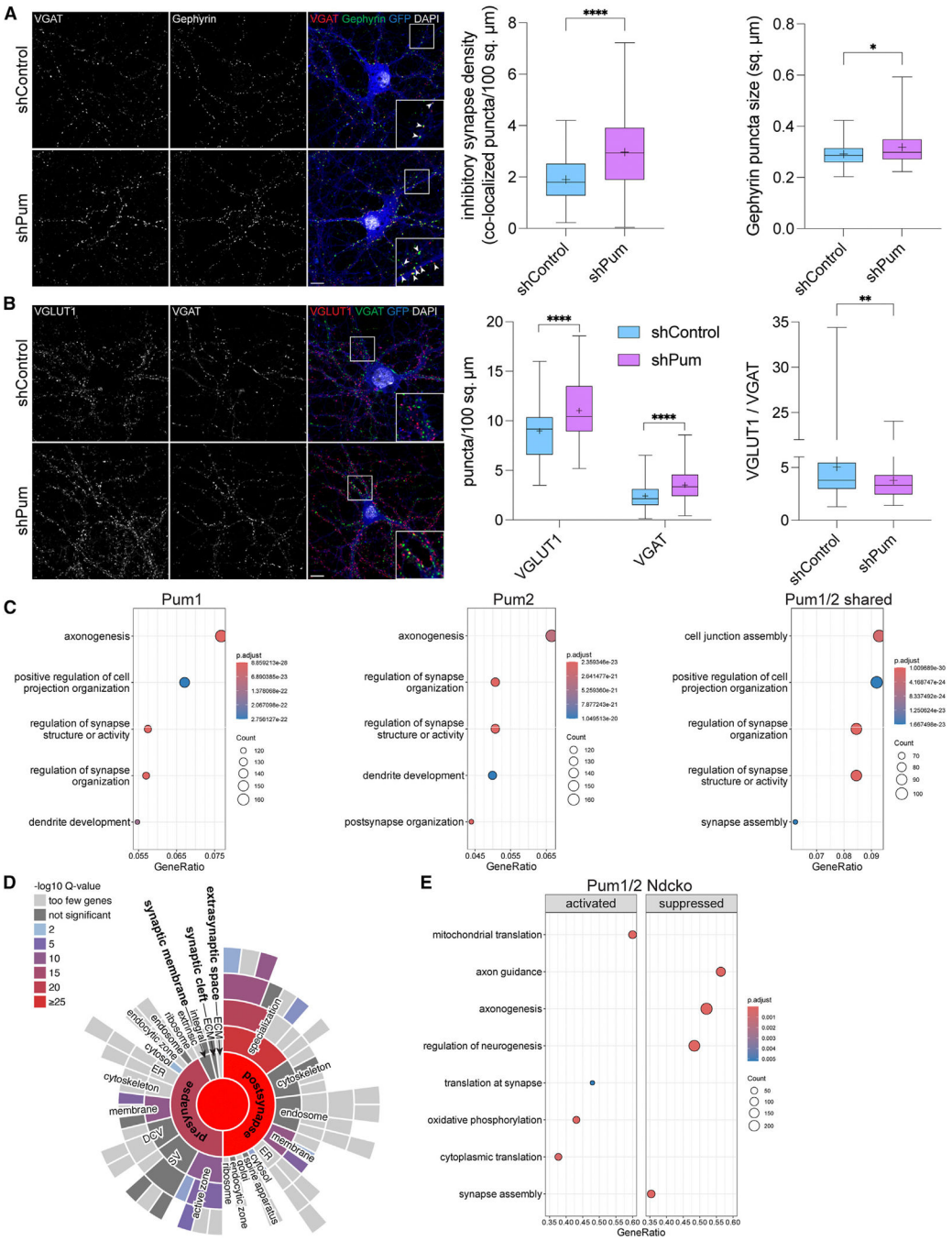

Figure 4. Pumilios regulate both excitatory and inhibitory synapses and control the expression of many synaptic genes

(A) Neurons infected on DIV1 with shControl or shPum lentiviruses were immunostained at DIV21 for VGAT and gephyrin. Arrows indicate co-localized VGAT+/gephyrin+ puncta (left). Quantification of inhibitory synapse count (center) and gephyrin puncta size (right) from $n = 80$ fields from 4 biological replicates, Mann-Whitney test.

(B) Neurons infected on DIV1 with shControl or shPum lentiviruses were immunostained at DIV21 for VGLUT1 and VGAT (left). Quantification of puncta count (center) and

Author Manuscript Author Manuscript Author Manuscript Author Manuscript

VGLUT1/VGAT ratio (right) from $n = 90–99$ fields per condition from 5 biological replicates, Mann-Whitney test.

(C) Gene Ontology analysis on neonatal mouse cortical brain iCLIP targets of Pum1, Pum2, or their intersection.

(D) SynGO analysis of the shared Pum1/2 targets from (C). Major gene categories are shown in bold, and subcategories are shown in regular type.

(E) Gene set enrichment analysis of RNA-seq data from conditional neural double knockout (*Nestin*-Cre-mediated, Ndcko) of Pum1 and Pum2 in mouse brain[18] showing suppression or activation of biological processes related to synaptic development, translation, and mitochondrial function.

(A and B) The total number of co-localized or individual puncta in a field was normalized to the area covered by the cell in the EGFP channel. Insets, 2× magnification. Scale bars, 10 μm. *$p < 0.05$, **$p < 0.01$, and ****$p < 0.0001$.

Author Manuscript Author Manuscript Author Manuscript Author Manuscript

KEY RESOURCES TABLE

REAGENT or RESOURCE	SOURCE	IDENTIFIER
Antibodies		
Rabbit anti-Pumilio 1 (WB 1:3000)	Abcam	Cat#ab92545; RRID:AB_10563695
Rabbit ant-Pumilio 1 (IP)	Bethyl	Cat#A302-567A; RRID:AB_2034852
Rabbit anti-Pumilio 2 (WB 1:1000; IP)	Bethyl	Cat#A300-202A; RRID:AB_2173752
Rabbit anti-SNAP-25 (WB 1:5000; PLA 1:500)	Millipore Sigma	Cat#S9684; RRID:AB_261576
Mouse anti-L1CAM (WB 1:1000)	Abcam	Cat#ab24345; RRID:AB_448025
Rabbit anti-Neurexin-1 (WB 1:1000)	Millipore Sigma	Cat#ABN161-I; RRID:AB_11211973
Mouse anti-Synaptotagmin-1 (WB 1:1000)	Synaptic Systems	Cat#105011; RRID:AB_887832
Mouse anti-β-III-tubulin (WB 1:5000)	Thermo Fisher Scientific	Cat#MA1-118; RRID:AB_2536829
Mouse anti-β-III-tubulin (WB 1:5000)	Abcam	Cat#ab7751; RRID:AB_306045
Alexa Fluor 488 conjugated mouse anti-β-III-tubulin (IF 1:500)	BioLegend	Cat#801203; RRID:AB_2564757
Mouse anti-Synapsin I (IF 1:500)	Synaptic Systems	Cat#106011; RRID:AB_2619772
Rabbit anti-PSD-95 (IF 1:200)	Cell Signaling	Cat#3450; RRID:AB_2292883
Rabbit anti-VGLUT1 (IF 1:1000)	Synaptic Systems	Cat#135303; RRID:AB_887875
Mouse anti-VGAT (IF 1:1000)	Synaptic Systems	Cat#131011; RRID:AB_887872
Mouse anti-Gephyrin (IF 1:250)	Synaptic Systems	Cat#147011; RRID:AB_887717
Rabbit anti-Gephyrin (IF 1:200)	Synaptic Systems	Cat#147008; RRID:AB_2619834
Chicken anti-MAP2 (IF 1:250)	Abcam	Cat#ab5392; RRID:AB_2138153
Mouse anti-Puromycin (PLA 1:1000)	Millipore Sigma	Cat#MABE343; RRID:AB_2566826
Bacterial and virus strains		
Escherichia coli: HST08 (Stellar™ Competent Cells)	Takara Bio	Cat#636766
AAV: AAV1-*syn*-jGCaMP8f	Zhang et al., 2023[61]	RRID:Addgene_162376
Chemicals, peptides, and recombinant proteins		
Puromycin	Thermo Fisher Scientific	Cat#A1113803; CAS:53-79-2
Anisomycin	Millipore Sigma	Cat#176880; CAS:22862-76-6
Latrunculin A	Tocris	Cat#3973; CAS:76343-93-6
Phalloidin-iFluor 647 (IF 1:1000)	Abcam	Cat#ab176759
Critical commercial assays		
Duolink® *in situ* PLA® probe anti-mouse PLUS	Millipore Sigma	Cat#DUO92001
Duolink® *in situ* PLA® probe anti-mouse MINUS	Millipore Sigma	Cat#DUO92004
Duolink® *in situ* PLA® probe anti-rabbit PLUS	Millipore Sigma	Cat#DUO92002
Duolink® *in situ* PLA® probe anti-rabbit MINUS	Millipore Sigma	Cat#DUO92005
Duolink® *in situ* detection reagents red	Millipore Sigma	Cat#DUO92008

Author Manuscript Author Manuscript Author Manuscript Author Manuscript

REAGENT or RESOURCE	SOURCE	IDENTIFIER
Duolink® *in situ* detection reagents far-red	Millipore Sigma	Cat#DUO92013
Direct-zol™ RNA MicroPrep kit	Zymo Research	Cat#R2060
Luna® Universal Probe One-Step RT-qPCR kit	New England Biolabs	Cat#E3006
Dynabeads™ M-280 Sheep Anti-Rabbit IgG	Thermo Fisher Scientific	Cat#11203D
In-Fusion® HD EcoDry Cloning Plus	Takara Bio	Cat#638913
QIAprep Spin Miniprep Kit	Qiagen	Cat#27104
ZymoPURE II Plasmid Midiprep Kit	Zymo Research	Cat#D4201
qPCR Lentivirus Titer Kit	Applied Biological Materials	Cat#LV900
Lenti-X™ Concentrator	Takara Bio	Cat#631231
Deposited data		
iCLIP-seq: Pum1 and Pum2 iCLIP from mouse brain	Zhang et al., 2017[18]	GEO:GSE95195
RNA-seq: Pumilio knockout in mouse brain	Zhang et al., 2017[18]	GEO:GSE95102
RNA-seq: mouse cortex across developmental stages	Weyn-Vanhentenryck et al., 2018[20]	SRA:PRJNA275412
Experimental models: Cell lines		
Human: HEK293T	ATCC	Cat#CRL-3216
Human: Lenti-X™ 293T	Takara Bio	Cat#632180
Experimental models: Organisms/strains		
Rat: Hsd:Sprague Dawley® SD®	Envigo	RRID:RGD_737903
Oligonucleotides		
Taqman gene expression assay (FAM): *Snap25*	Thermo Fisher Scientific	Cat#4331182; Rn00578534_m1
Taqman gene expression assay (FAM): *L1cam*	Thermo Fisher Scientific	Cat#4331182; Rn00493049_m1
Taqman gene expression assay (FAM): *Syt1*	Thermo Fisher Scientific	Cat#4331182; Rn00436862_m1
Taqman gene expression assay (FAM): *Nrxn1*	Thermo Fisher Scientific	Cat#4331182; Rn00665869_m1
Taqman gene expression assay (FAM): *Pum1*	Thermo Fisher Scientific	Cat#4331182; Rn01180594_m1
Taqman gene expression assay (FAM): *Pum2*	Thermo Fisher Scientific	Cat#4331182; Rn01469425_m1
Taqman gene expression assay (FAM): *Rps19*	Thermo Fisher Scientific	Cat#4331182; Rn01458091_g1
Recombinant DNA		
Plasmid: pZIP-hUbC-eGFP-shControl	transOMIC Technologies; modified in-house	N/A
Plasmid: pZIP-hUbC-ZsGreen1-shControl	transOMIC Technologies; modified in-house	N/A
Plasmid: pZIP-hUbC-mLumin-shControl	transOMIC Technologies; modified in-house	N/A
Plasmid: pZIP-hUbC-eGFP-shPum1	transOMIC Technologies; modified in-house	N/A
Plasmid: pZIP-hUbC-ZsGreen1-shPum1	transOMIC Technologies; modified in-house	N/A
Plasmid: pZIP-hUbC-eGFP-shPum2	transOMIC Technologies; modified in-house	N/A

Author Manuscript Author Manuscript Author Manuscript Author Manuscript

REAGENT or RESOURCE	SOURCE	IDENTIFIER
Plasmid: pZIP-hUbC-ZsGreen1-shPum2	transOMIC Technologies; modified in-house	N/A
Plasmid: pZIP-hUbC-eGFP-shPum	transOMIC Technologies; modified in-house	N/A
Plasmid: pZIP-hUbC-ZsGreen1-shPum	transOMIC Technologies; modified in-house	N/A
Plasmid: pZIP-hUbC-mLumin-shPum	transOMIC Technologies; modified in-house	N/A
Plasmid: pZIP-hUbC-shPum1-shPum2	transOMIC Technologies; modified in-house	N/A
Plasmid: FUGW	Lois et al., 2002[62]	RRID:Addgene_14883
Plasmid: hUbC-Pum1^{R}	Expression of mouse Pum1 CDS replacing eGFP in FUGW with silent mutations of serine 1113 through threonine 1117 in shPum-targeting site (AG**T** GC**C** TT**A** TA**C** AC**C** to AG**C** GC**G** TT**G** TA**T** AC**G**; translation is preserved)	N/A
Plasmid: hUbC-Pum2^{R}	Expression of mouse Pum2 CDS replacing eGFP in FUGW with silent mutations of serine 990 through threonine 994 in shPum-targeting site (AG**T** GC**C** TT**A** TA**C** AC**C** to AG**C** GC**G** TT**G** TA**T** AC**G**; translation is preserved)	N/A
Plasmid: pCMVΔ R8.9	Lois et al., 2002[62]	N/A
Plasmid: pHCMV VSVg	Lois et al., 2002[62]	N/A
Software and algorithms		
GraphPad Prism 9 (version 9.4.0)	GraphPad	https://www.graphpad.com/features
ImageJ (Fiji)	Schindelin et al., 2012[63]	https://imagej.net/
Puncta Analyzer	Ippolito & Eroglu, 2010[21]	https://sites.duke.edu/eroglulab/tools/
Bedtools (version 2.30.0)	Quinlan & Hall, 2010[64]	https://github.com/arq5x/bedtools2
SynGO (version 1.2)	Koopmans et al., 2019[29]	https://www.syngoportal.org/
Salmon (version 1.10.1)	Patro et al., 2017[65]	https://combine-lab.github.io/salmon/
R (version 4.3.2)	R Core Team	https://www.r-project.org/
clusterProfiler (v4.10.0)	Yu et al., 2012,[66] and Wu et al., 2021[67]	https://bioconductor.org/packages/release/bioc/html/clusterProfiler.html
tximport (version 1.30.0)	Soneson et al., 2016[68]	https://bioconductor.org/packages/release/bioc/html/tximport.html
Limma-Voom (version 3.58.1)	Ritchie et al., 2015,[69] and Law et al., 2014[70]	https://bioconductor.org/packages/release/bioc/html/limma.html
AnnotationDbi (version 1.64.1)	Pagès et al., 2023[71]	https://bioconductor.org/packages/release/bioc/html/AnnotationDbi.html
org.Mm.e.g.,.db (version 3.18.0)	Carlson 2023[72]	https://bioconductor.org/packages/release/data/annotation/html/org.Mm.eg.db.html
dplyr (version 1.1.4)	Wickham et al., 2023[73]	https://cran.r-project.org/web/packages/dplyr/index.html
tidyr (version 1.3.1)	Wickham et al., 2024[74]	https://cran.r-project.org/web/packages/tidyr/index.html

Author Manuscript Author Manuscript Author Manuscript Author Manuscript

REAGENT or RESOURCE	SOURCE	IDENTIFIER
pheatmap (1.0.12)	Kolde 2019[75]	https://cran.r-project.org/web/packages/pheatmap/
ggplot2 (3.5.1)	Wickham 2016[76]	https://cran.r-project.org/web/packages/ggplot2/index.html
Code used for RNAseq and iCLIP analysis	This Paper	https://github.com/jcmtnez/2024-Cell_Reports-Randolph_et_al https://zenodo.org/records/12816566